PERIODIC PULSATION IN LEAN PREMIXED COMBUSTORS AND NONLINEAR DYNAMICAL SYSTEMS

A Thesis

by

JACOB QUENTIN DOLL

Submitted to the Office of Graduate and Professional Studies of
Texas A&M University
in partial fulfillment of the requirements for the degree of

MASTER OF SCIENCE

Chair of Committee,	Adonios Karpetis
Committee Members,	John Hurtado
	Eric Petersen
Head of Department,	Rodney Bowersox

December 2019

Major Subject: Aerospace Engineering

ABSTRACT

Lean-premixed combustors have seen increased use due to the combined benefits of increased fuel efficiency and reduced pollutant emissions; however, these systems are prone to combustion instabilities and flashback. We have analyzed the dynamical behavior of one particular type of instability – which we refer to as periodic pulsation – using a reduced-order combustion model for lean-premixed combustors. From the combustion model we have established a set of criteria for the appearance of periodic pulsation, and we have demonstrated that applying similar conditions to two other dynamical systems (including the Van der Pol oscillator) produces the periodic pulsation phenomenon in those systems. The phenomenon is distinguished by regular pulses of high-amplitude oscillation in time separated by periods of relative calm – visually similar to an ultrashort pulse found in nonlinear optics. Although every pulse repeats periodically from a macroscopic point of view, we have shown that the state space trajectory behavior of periodic pulsation must inherently be quasi-periodic – regardless of the dynamical system in question. We have found that under certain conditions the trajectories of periodic pulsation can resemble the ECG signal of heartbeats; furthermore, the two systems studied besides the combustion model can exhibit what is best described as 'arrhythmias' in the periodic pulsation signal.

DEDICATION

To my parents, for their continued love and support of all my endeavors.

And to all my friends on the Sounding Rocketry Team, for all the good times that I will never forget, and for going 523ft higher than we've ever gone before.

ACKNOWLEDGMENTS

I would like to thank the Texas A&M Department of Aerospace Engineering and College of Engineering for everything that I have learned in both my undergraduate and graduate education. Special thanks to Dr. Adonios Karpetis, Dr. John Hurtado, and Dr. Eric Petersen for carefully reviewing this material.

Support by ARL through grant M1703539, (BryanGlaz, manager) is gratefully acknowledged.

CONTRIBUTORS AND FUNDING SOURCES

Contributors

This work was supported by a thesis committee consisting of Professor Adonios Karpetis [advisor] and Professor John Hurtado of the Department of Aerospace Engineering, and Professor Eric Petersen of the Department of Mechanical Engineering.

All work conducted for the thesis was completed by the student independently.

Funding Sources

Graduate study was supported by a grant from the U.S. Army Research Laboratory (ARL).

NOMENCLATURE

A	Forcing amplitude
A_{bif}	Amplitude at which an arrhythmia bifurcation occurs
B	Sine forcing term: $\sin(2\pi t/\tau)$
CFD	Computational Fluid Dynamics
d	Distance between trajectory and central fixed point
DFT	Direct Fourier Transform
f	Frequency in Hertz
k	Arrhythmia constant
LTI	Linear Time-Invariant (differential equation)
LTV	Linear Time-Variant (differnetial equation)
Q	Charge in the Van der Pol Oscillator circuit
R	Resistance in the Van der Pol Oscillator circuit
SHB	Simple Hopf Bifurcation (Model)
T	System temperature
T_0	Temperature of the outside of the combustion chamber wall
U	Current in the Van der Pol Oscillator Circuit
VDP	Van der Pol (Oscillator)
X	Concentration of the radical species
x	State parameter in the Simple Hopf Bifurcation Model
α	Frequency ratio: $\omega_{fast}/\omega_{slow}$
λ	Characteristic value of a fixed point
μ	Control parameter in the Simple Hopf Bifurcation Model

ϕ	Arrhythmia angle
τ	Forcing period
ω_n	Natural frequency of a system in rad/s

TABLE OF CONTENTS

Page

LIST OF FIGURES

FIGURE Page

LIST OF TABLES

TABLE Page

CHAPTER 1

INTRODUCTION

The phenomenon we refer to as periodic pulsation is distinguished by regular pulses of high-amplitude oscillation in time separated by periods of low-amplitude (or practically zero amplitude) – visually similar to an ultrashort pulse found in nonlinear optics [2], as well as ECG signals of heartbeats (under certain conditions). Periodic pulsation has been observed as a combustion instability in at least two experiments related to lean premixed combustors. This is important because lean premixed combustors have seen increased use in jet engines and power generation turbines due to the combined benefits of increased fuel efficiency and reduced pollutant emissions; however, these systems are more prone to combustion instabilities – such as periodic pulsation – and flashback [3, 4]. The first experiment was by Hong *et al.*, in which the test apparatus was a lean-premixed swirl combustor burning LPG and air [1]. Although this particular fuel-oxidizer combination is not widely used in jet engines (especially at ambient operating pressure), the experiment remains relevant to certain combustors and gas turbines. The second experiment was by Fanglong Weng, Min Zhu, and Liyue Jing, in which periodic pulsation (what they referred to as "beating") was observed in premixed Rijke burners [5, 6].

Our work up to this point has shown that periodic pulsation is driven by a slow periodicity on the damping/dissipation mechanism of a given nonlinear dynamical system, but in conjunction with a Hopf bifurcation. The exact dissipation mechanism responsible for the pulsation signal seen in the Hong *et al.* experiment remains undetermined, but the pulsation signal of the second experiment by Weng, Zhu, and Jing was determined to be a slow periodicity on the heat loss (a dissipation mechanism) due to the shape of the flame [6]. We suspect the same type of heat loss mechanism is causing the periodic pulsation of the swirl combustor in the Hong *et al.* experiment. Additionally, we believe that the heat loss in that case is also coupled with the chemical kinetics of the combustion of propane, as propane can exhibit intermediate cool flame behavior under lean-burning conditions [7, 8]. We know from the first experiment that the observed pulses in

pressure correspond to different flame behaviors – pulses when the flame is bound in the ring vortex generated from recirculation, and calm periods when the flame lifts off straight from the injector face [1]. In essence, our idea is that the chemical reaction proceeds towards the high-temperature branch (in reference to Semenov branching), heat loss through the walls increases and drives the temperature back down. Then the reaction drives the temperature back up and the cycle repeats. This type of oscillation – where heat loss and chemical kinetics are the driving factors – has been shown in a model for cool flames of general hydrocarbons by Yang & Gray [9]. This model will serve as an initial combustion model to study periodic pulsation from a dynamics standpoint, and will allow us to develop general criteria for the appearance of periodic pulsation in nonlinear dynamic systems.

One of the other goals of this research was to try to model the pulsation seen in the Hong *et al* experiment through computational fluid dynamics (CFD) simulation. The time-varying nature of the pulsation required that the simulation be fully transient, but a sort of 'saving grace' in terms of dimensionality was the fact that the experiment used a cylindrical combustion chamber with an annular injector. This implies that we can apply an axisymmetric assumption to reduce the dimensionality from (3D+time) to (2D+time). Our initial computations use a relatively simple combustion mechanism for methane in order to gain some insight into producing periodic pulsation in our simulations. So far we have been able to generate only a single pulse (likely due only to transients in the solution steps), but even this gives us information as we proceed to more complex chemical mechanisms.

The criteria for periodic pulsation developed in the Combustion model led us to two more nonlinear dynamical systems that could exhibit periodic pulsation. The first (and simplest) one was found in Hilborn's text on nonlinear dynamics and chaos [10]. We will refer to the system as the Simple Hopf Bifurcation (SHB) model. Utilizing the criteria from the Combustion model, periodic pulsation can be produced in the SHB. In fact, the SHB can exhibit more rich dynamical behavior than the Combustion model – an example of which is best described as an "arrhythmia" bifurcation. This particular system was simply meant to model a limit cycle/ Hopf bifurcation, and

as such it does not necessarily have a direct physical analogue.

The second nonlinear dynamical system we studied is the Van der Pol oscillator (VDP), one of the most thoroughly studied relaxation oscillators; however, instead of adding a forcing term to the end of the equations – as Van der Pol himself studied [11] – the forcing term is added to the control parameter (as with the previous models) and periodic pulsation can be produced. The specific form of the Van der Pol oscillator equation we used was also used in Hilborn's nonlinear dynamics text [10]; however, the normal form of the equation could also be used, albeit with forcing placed in the proper position in the equation. The arrhythmia bifurcation described in the SHB model can also be produced in the Van der Pol oscillator – but with one slight difference. One interesting note is that although the SHB did not have a direct physical representation, the VDP is based directly on an actual electrical circuit – implying that this circuit might be able to produce periodic pulsation in reality with the proper type of resistance/damping.

Although we refer to the phenomenon as periodic pulsation (due to the periodic behavior of characteristic values that cause the pulsation, and the visual periodicity of pulses), the trajectory behavior for each of the dynamical systems studied here is generally quasi-periodic – barring arrhythmias. This is evidenced by the existence of drift rings in the Poincaré planes of periodic pulsation signals, as well as the shapes of frequency spectra in the Discrete Fourier Transforms (DFT) of periodic pulsation signals.

While studying each of the three nonlinear dynamic systems in this work, it became apparent that a relatively simple function can reproduce periodic pulsation – which we be rightfully called the "Pulsation Function". Although producing even a steady-state closed form solution for any of the previous three systems using the function proved fruitless, the function itself serves as the simplest form of pulsation that was found. Along similar lines, we were also able to produce periodic pulsation in the simple spring-mass-damper system (with its own peculiar issues), although that system could not be solved using the Pulsation Function, either.

CHAPTER 2

PERIODIC PULSATION IN A LOW-ORDER COMBUSTION MODEL

In what follows, we describe the basics of the experiment by Hong *et al.* that exhibited periodic pulsation, and subsequently we present a possible model based on cool flame behavior that may explain the experimental observations. Our model has reduced dimensionality and reduced chemical kinetics, yet presents complex dynamics and interesting heat behavior.

2.1 Background for the Combustion Model

2.1.1 An experiment by Hong *et al.*

A recent experimental work by Hong *et al.* [1] examined a premixed propane/air swirl burner that produced a broad taxonomy of dynamics. The burner consisted of a pre-combustion plenum where the fuel – liquified petroleum gas, treated as propane – and the oxidizing air were premixed before entering the 700-mm long combustor proper which had optical access. The burner had a backward-facing step configuration to enhance mixing and flame-holding, both of which were also supported by the presence of swirl. The fuel supply could operate in either choked or unchoked mode, with the latter being more significant for the experiment since it resulted in an oscillatory flow condition at the entrance of the burner. [This oscillatory behavior can be seen in Fig. 2.1, and is characterized not only by an intermittent/pulsing behavior in the pressure fluctuation, but also by the switching of flame modes between one state where the flame is "wrapped up" around the outer ring vortex caused by the backward facing step, and another state where the flame has "lifted off" away from the injector face. Also, the first flame mode (around the ring vortex) corresponded with the periods of large pressure fluctuation, and the the second flame mode (lifted off from the injector face) corresponded to the periods of little to no pressure fluctuation.]

This behavior, termed "quasi-periodic intermittency" by Glaz and co-workers [12], and which we call periodic pulsation, incorporates both long and short timescale flame fluctuations. This type of intermittent/pulsing behavior has been identified in fluid mechanical systems [12], lasers [13],

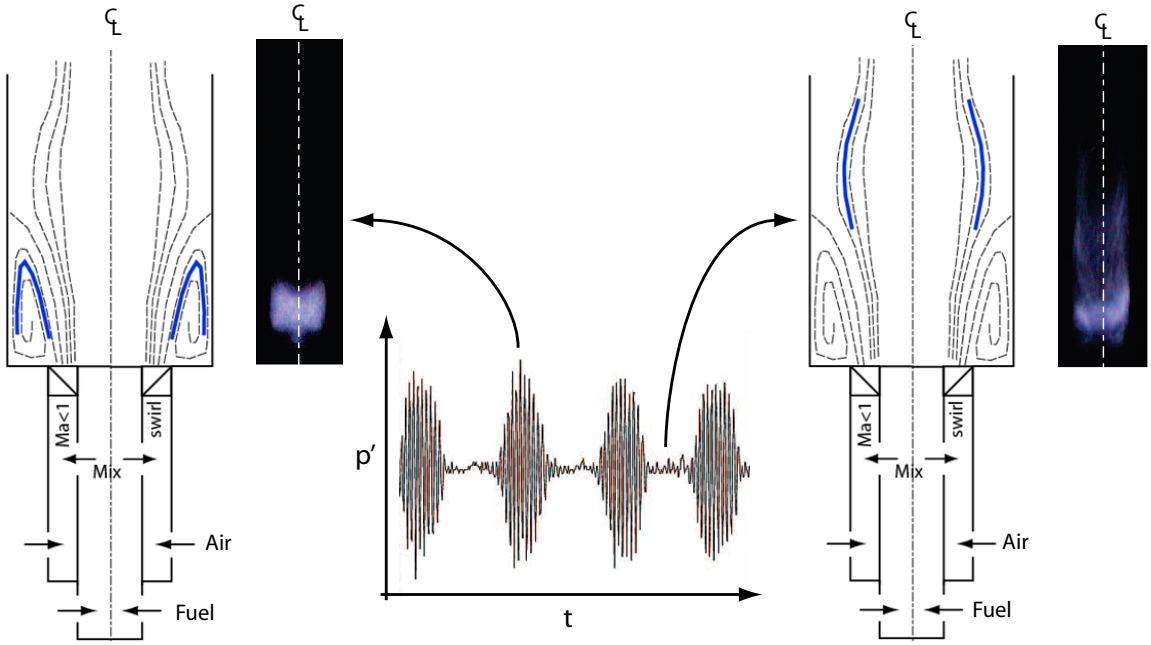

Figure 2.1: Propane/air swirl burner of [1]. Images at left show a flame anchored at the base of the burner or the top of the burner (Mode 1 and 4 respectively); Images at right show Type-II (Mode 2) intermittency and equivalent pressure fluctuations.

catalytic reactors [14], and burners [1, 5, 6].

2.1.2 Reduced-Order Model Based on Cool Flames

While the short time fluctuations seen in Hong *et al.* can be unequivocally attributed to the pressure fluctuations at the burner inlet, the cause of the long timescale fluctuation is not clearly known [1]. Identifying the driving force behind this behavior is one of the main objectives of our current work. Emphasis will be placed on 'cool flame' type of phenomena which result in long time fluctuations in chemically reacting systems with higher hydrocarbon (HC) fuels, i.e. propane or heavier [15]. Cool flame experiments were introduced by Newitt and Thornes in 1937 [7] and were connected to the chemical branching theory developed by Semenov [16, 17] and to the 'explosion limits' of higher hydrocarbons [18].

Cool flames are considered a prototypical/canonical problem in chemical kinetics, at least in its simplified form. Semenov [16] described temperature-sensitive chemical kinetics that would switch behavior at some (low) temperature from a branching chemical reaction with low activation

energy (Reaction II) to a non-branching chemical reaction with high activation energy (Reaction I) at some intermediate temperature. The transition from Reaction II to Reaction I was termed "degenerate branching," and is thought of as the 'heart' of HC oxidation, i.e. the balance between two kinetic routes, one a low temperature and the other a high temperature mechanism that can be used to explain the three H2/O2 explosion limits – and HC explosion limits more generally – as well as the "Negative Temperature Coefficient" (NTC) behavior at intermediate temperatures of HC oxidation [18]. The two kinetic routes for the degenerate branching of Reactions I and II is shown in Fig. 2.2 below.

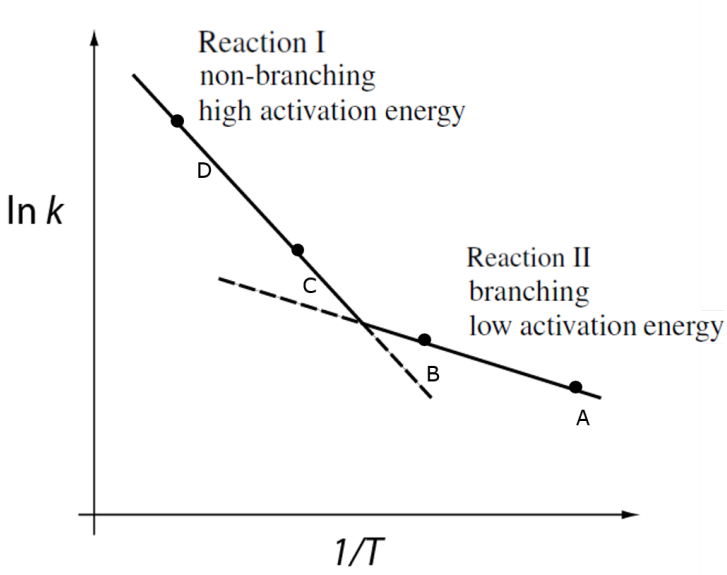

Figure 2.2: Diagram showing the two kinetic routes for Semenov's degenerate branching of Reaction I and Reaction II.

At low temperatures Reaction II – the low activation energy chemical branching – dominates and leads to a chemical "runaway" and temperature increase due to its exothermicity; as the temperature increases the system crosses over to Reaction I, the high activation energy non branching (propagating) exothermic step that leads to thermal runaway and further temperature increase. The overall phenomenon occurs at low to intermediate temperatures and results in a modest temper-

ature increase (e.g. 200 ^{o}C [15]). In order for the process to repeat itself, and a cool flame to be established, a restoring heat loss mechanism must be present such that the temperature of the system is reduced, Reaction II again becomes prominent, and the system becomes explosive again by virtue of the chemical runaway [18]. In an actual experiment (such as Ref. [7]) this cool flame phenomenon cycles for a few times – anywhere from 2-6 depending on the fuel composition – with a long timescale that depends on the system size and the details of the heat loss mechanism.

A calculation of a simplified, minimal system that exhibits cool flame type of behavior has been set up analytically, following published work by Liñán and coworkers. They, in turn, set up their system of reactions following the work of Yang and Gray [9] which was the first to show a repeatable oscillatory dynamics in a four-step reaction system. In what follows we use the somewhat archaic nomenclature and system of units of the original work.

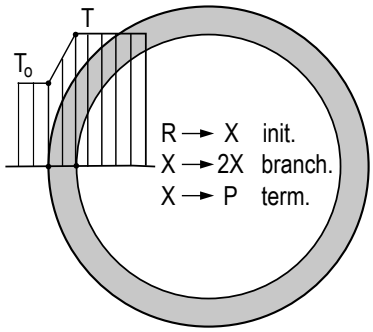

Figure 2.3: A simple diagram for the geometry of the combustion chamber used in the Yang & Gray model.

Values of constant pressure p_o = 480 mm Hg, and initial/boundary temperature of T_o = 560 K were used in the calculations. These values are important, insofar as they correspond to the 'intermediate' temperature range of hydrocarbon oxidation, and also to the conditions of Hong *et al.* The subatmospheric pressure is also important for what follows, as it sets up realistic rates for the reactions that do not conserve moles (volume) between reactants and products. The vessel diameter is set equal to d = 4 cm and the conductivity to $\lambda = 1.4\times10^{-4}$ cal/(cm K sec). The universal gas con-

stant $\bar{R}$ = 2 cal/mol/K corresponds to molar density of ideal-gas species of N_o=4.467$\times 10^{-5}$ mol/cc.

Some further parameters were postulated in the original study: Heat capacity c_v = 11$\times N_o$ cal/cc/K, and a "heat transfer" coefficient Γ = 21.6, which, when multiplied by $\sim (T - T_o)/d^2$ would result in the Fourier heat flux for a cylindrical vessel of diameter d. Recognizing that we need to evaluate the terms in mass (species) conservation equations, as well as the energy equation, we must make an equidiffusive system approximation for mass and energy diffusivities, D and α respectively [18]:

$$D = \alpha = \lambda/(\rho c_p) = \lambda/[p_o(c_v + R)/(\bar{R}T/MW)]$$

Assuming a value of average molecular weight MW = 10 allows us to evaluate mass and energy diffusion terms proportional to a coefficient Δ = c $\Gamma D/d^2$ = c $\Gamma\alpha/d^2$. [1] Future work will examine the effect of mass diffusion on the dynamics of the chemical system; for now only the heat transfer will be considered as a 'restoring force' to the thermal runaway of the non-branching reaction.

The four chemical steps to consider, as well as the Arrhenius rates for each reaction, are:

Initiation(i)	$R \rightarrow X$	$k_i = A_i N_o^2 \exp(-E_i/\bar{R}T(t))$
Branching(b)	$X \rightarrow 2\,X$	$k_b = A_b N_o \exp(-E_b/\bar{R}T(t))$
Termination(t1)	$X \rightarrow P1$	$k_{t1} = A_{t1} N_o^{1/2} \exp(-E_{t1}/\bar{R}T(t))$
Termination(t2)	$X \rightarrow P2$	$k_{t2} = A_{t2} N_o \exp(-E_{t2}/\bar{R}T(t))$

where R and P1, P2 are stable reactant and product species, while X is an intermediate radical species that participates in all reactions from initiation to branching and termination. The minimum set of reactions needed to create an oscillatory cool flame behavior is three, namely initiation (i), branching (b), and termination (t). Two termination reactions were used in the original study [9] in order to explain the behavior of the system with different initial temperatures. This 4-step formulation is used here for the same purpose, i.e. physical realism of the system. The 3-step

[1] The constant c is inserted as a parameter, of order 1, that will be varied to explore the dynamics of the thermo-chemical system. Values of c in the range [0.8695-3] resulted in a limit cycle behavior, while values outside this range did not. In everything that follows the parameter is set to unity ($c = 1$).

Table 2.1: Arrhenius and thermal parameters for a minimal system that exhibits cool flame behavior

Reaction	Pre-exp A	Activation E (cal/mol)	Heat rxn (cal/mol)
(i)	1.60×10^{10}	2.4×10^{4}	0
(b)	1.38×10^{8}	7.0×10^{3}	7×10^{3}
(t1)	$3.30 \times 10^{3}/d$	0	0
(t2)	7.80×10^{10}	1.6×10^{4}	4×10^{2}

reduced system can also exhibit dynamics akin to periodic pulsation, and can be used instead for purposes of analytical calculations.

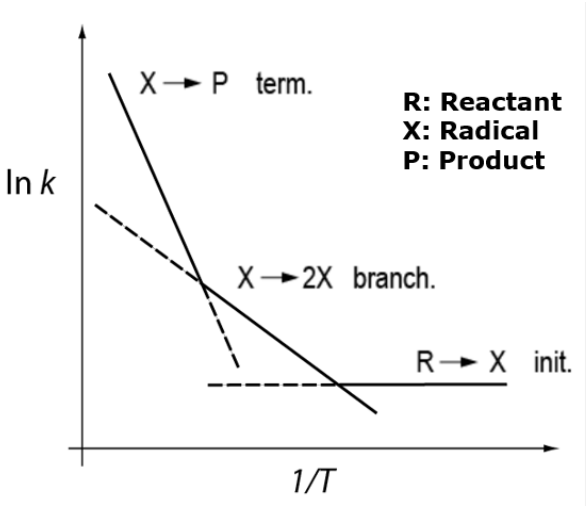

Figure 2.4: Kinetic routes for the chemical mechanism of the Yang & Gray model for cool flames in general hydrocarbons.

The terms above have an Arrhenius-like form, but they are written with the pre-exponential temperature power-law dependence appearing as a concentration power. This form does not conform with the ones found in more modern publications, insofar as the units of the pre-exponential constants are complicated, and only the initial boundary temperature, T_o, or its surrogate concentration, N_o, shows up in the pre-exponential term. The exponents of concentration N_o appearing in the reaction rates have been chosen by the authors of the original study in such a way as to

optimize the appearance of cool flame dynamics; still, they can be rationalized with recourse to actual initiation, branching and termination reaction rates for hydrocarbon oxidation. Values for some constants are given in Table 2.1.

Finally, the two equations describing the thermal and chemical dynamics of the system are:

$$\frac{dT}{dt} = [k_i h_i + (k_{t1} h_{t1} + k_{t2} h_{t2} + k_b h_b)X - \Gamma(T - T_o)/d^2]/c_v \tag{2.1}$$

$$\frac{dX}{dt} = k_i - (k_{t1} + k_{t2} - k_b)X \tag{2.2}$$

where the concentration of radical species X (in mol/cc) and the temperature T are both functions of time. In order to reproduce the original result of an oscillatory system that mimics the cool flame phenomenon with heat conduction alone, the species equation (Eq. 2.2) was written without a mass diffusion term which can be trivially included in the calculation.

As will be shown subsequently this minimal system is sufficient to generate an oscillatory dynamics simply by the inclusion of four (or three) reaction rates. A stable limit cycle can be seen in the phase plot of X and T in Fig. 2.5a consistent with the original ideas by Semenov regarding the intermediate temperature behavior of hydrocarbon oxidation. The characteristic timescale of the chemical oscillation corresponds to a fast timescale that can be controlled by changing the thermodynamic and geometric parameters of the system (volume, temperature, density, etc.)

As we will see later, in order to introduce a pulsation in the oscillatory dynamics, a second, slow timescale may be postulated to be active through the heat conduction term $\Gamma(T - T_o)/d^2$. This is, of course, an *ad hoc* method, but does not lack physical significance: the temperature at the boundary of the vessel (bath) may well be oscillatory in nature, and the timescale of any such phenomenon (τ) is expected to scale with a "diffusion" type scaling:

$$d^2 \sim \alpha\tau$$

where α is the thermal diffusivity and d the vessel diameter.

2.2 Thermokinetic Model without Forcing

To reiterate, the Yang & Gray model breaks the combustion process into four sub-reactions – one initiation reaction, one branching reaction, and two termination reactions – with a radical species, X, acting as an intermediate between the reactants and products. The model is a set of two first-order nonlinear differential equations describing the system energy and chemical kinetics of the reaction, with the reaction temperature, T, and the concentration of the radical of the branching reaction, X, being the two state variables of the system. In this system of equations T_0 is the control parameter, and its effects on the dynamics are of critical importance to the periodic pulsation phenomenon (as we shall see). For simplicity, we can write the system of equations as a vector function, $\vec{f}$:

$$\vec{f}(T,X) = \begin{cases} f_1 = \dfrac{dT}{dt} = \frac{1}{c_v}\Big(k_i h_i + (k_{t1}h_{t1} + k_{t2}h_{t2} + k_b h_b)X - \frac{\Gamma\lambda}{d^2}(T - T_0)\Big) \\ f_2 = \dfrac{dX}{dt} = k_i - (k_{t1} + k_{t2} - k_b)X \end{cases} \tag{2.3}$$

Our analysis of the dynamics of this system of equations begins with determining its fixed points, which requires setting the function $\bar{f}(T,X)$ equal to 0 and solving for the corresponding fixed points T* and X* that satisfy that system. In other words, we evaluate the the equilibrium condition of the system:

$$\bar{f}(T^*, X^*) = 0 \tag{2.4}$$

In the equilibrium system above, the species equation can be rearranged, which immediately gives one of the system's fixed points by setting $T^* = T_0$:

$$X_1^* = \frac{k_i(T_0)}{k_{t1}(T_0) + k_{t2}(T_0) - k_b(T_0)} \tag{2.5}$$

The other fixed point of the system is obtained numerically using the Jacobian matrix of the

system, [J], given by:

$$[J] = \begin{bmatrix} \dfrac{\partial f_1}{\partial T} & \dfrac{\partial f_1}{\partial X} \\ \\ \dfrac{\partial f_2}{\partial T} & \dfrac{\partial f_2}{\partial X} \end{bmatrix} \tag{2.6}$$

which is also used in evaluating the characteristic values of each fixed point. The characteristic values, λ, of a fixed point determine the behavior of state space trajectories near that fixed point, and are determined by solving for the eigenvalues of the Jacobian matrix evaluated at each fixed point.

$$\det([J^*] - \lambda[I]) = 0, \qquad [J^*] = \begin{bmatrix} \left.\dfrac{\partial f_1}{\partial T}\right|_{(T^*,X^*)} & \left.\dfrac{\partial f_1}{\partial X}\right|_{(T^*,X^*)} \\ \\ \left.\dfrac{\partial f_2}{\partial T}\right|_{(T^*,X^*)} & \left.\dfrac{\partial f_2}{\partial X}\right|_{(T^*,X^*)} \end{bmatrix} \tag{2.7}$$

The above equation yields two characteristic values for each fixed point. The first fixed point at (T_0, X_1^*) has two real characteristic values of opposite sign, corresponding to a saddle point. The characteristic values of the second fixed point (T^*, X_2^*) form a complex conjugate pair, corresponding to either a spiral node or spiral repellor depending on the sign of the real part, σ.

Table 2.2: Fixed Points and Their Characteristic Values

Fixed Point	λ_1	λ_2	Attractor
(T_0, X_1^*)	+	-	Saddle Point
(T^*, X_2^*)	$\sigma + \omega j$	$\sigma - \omega j$	Sp. Node or Lim. Cycle

The second fixed point is of particular interest, as it has a greater effect on the overall trajectory behavior of the system during periodic pulsation. Depending on the value of the control parameter, T_0, the second fixed point is either a spiral repellor paired with a limit cycle or a spiral node. In fact, when $T_0 \lesssim$ 578K, the fixed point is spiral repellor ($Re(\lambda) > 0$) and a limit cycle is born around

it; when $T_0 \gtrsim$ 578K, the fixed point is a spiral node ($Re(\lambda) < 0$). In short this system exhibits a Hopf bifurcation. A Hopf bifurcation is a type of bifurcation where, as the control parameter is varied, the behavior of a given fixed point abruptly switches from a spiral node to a spiral repellor enclosed by a limit cycle. The value of the control parameter where the switch occurs is simply called the Hopf bifurcation point. In our case, the attractor switches from a limit cycle (with a spiral repellor) to a spiral node at the bifurcation point of $T_0 \simeq$ 578K. The two attractors of the system can be seen in Figure 2.5a and Figure 2.5b.

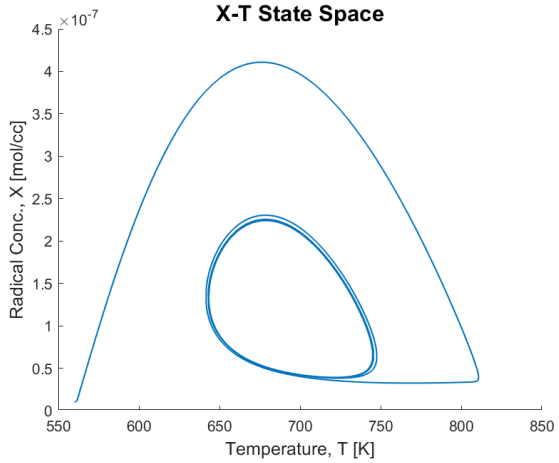

(a) $T_0 < 578K$: State Space

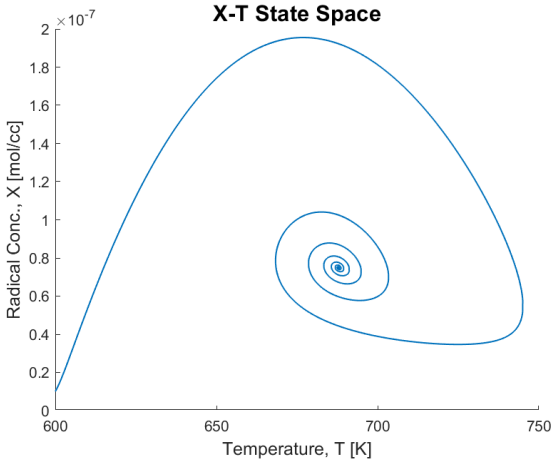

(b) $T_0 > 578K$: State Space

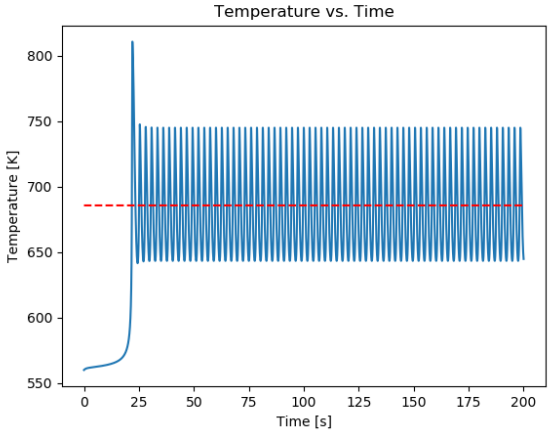

(c) $T_0 < 578K$: Temperature vs. Time

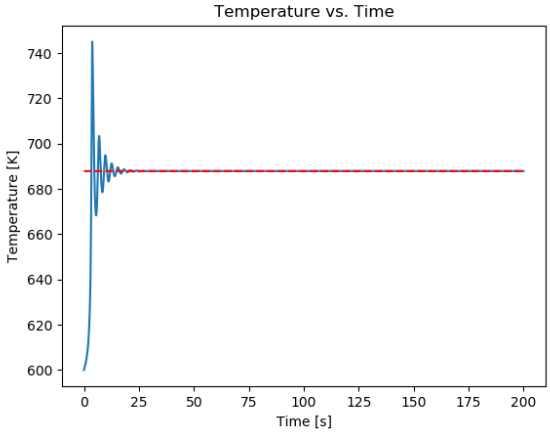

(d) $T_0 > 578K$: Temperature vs. Time

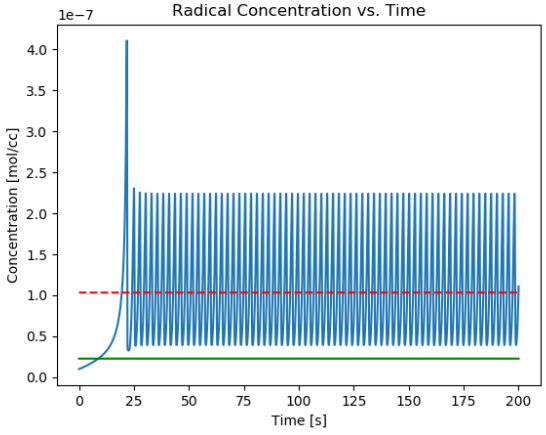

(e) $T_0 < 578K$: Concentration vs. Time

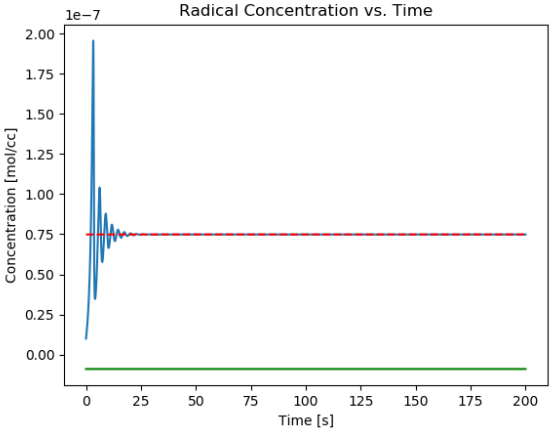

(f) $T_0 > 578K$: Concentration vs. Time

Figure 2.5: Trajectory and Attractor behavior with varied T_0.

On each of the bottom two plots of Figure 2.5, the green line represents the first fixed point of the system (with two real characteristic values), and the red dashed line represents the second fixed point of the system (with a complex conjugate pair of characteristic values). The left-hand set of plots shows the limit cycle attractor (when the fixed point is a spiral repellor), and the right-hand plots show the spiral node attractor.

This mathematical behavior mimics the underlying kinetics: the reduced chemistry represented by Eqn. 2.3 – with the associated physical and geometrical parameters of the system – captures the basic intermediate behavior HC at 600K. The explosion limit curves (thermal, chemical, etc.) of this system are well documented by Yang & Gray, and as such the limits on the control parameter/boundary condition temperature T_0 are between $\sim$560K and $\sim$675K [9]. In other words, if T_0 is set outside of these limits, then the system will fall outside of the explosion limit curves determined by Yang & Gray at some point in the time-evolution of the state space trajectory.

2.3 Thermokinetic Model with Forcing

Now we add a slow periodic forcing on the boundary condition temperature T_0. A diagram for how this forcing is being implemented is given in below. The physical picture corresponds to heat conduction through the vessel wall, from the hot interior to the colder surroundings, with the added complication of an oscillatory condition for the temperature at the external wall. While this simple physical picture is not particularly realistic, it may correspond adequately to more complicated geometries, like the one show in Fig. 2.1. The recirculation "bubble" seen at the side of the backward-facing step of the burner inlet may be thought of as a region that exposes the premixed reactants to an alternating/oscillating temperature boundary.

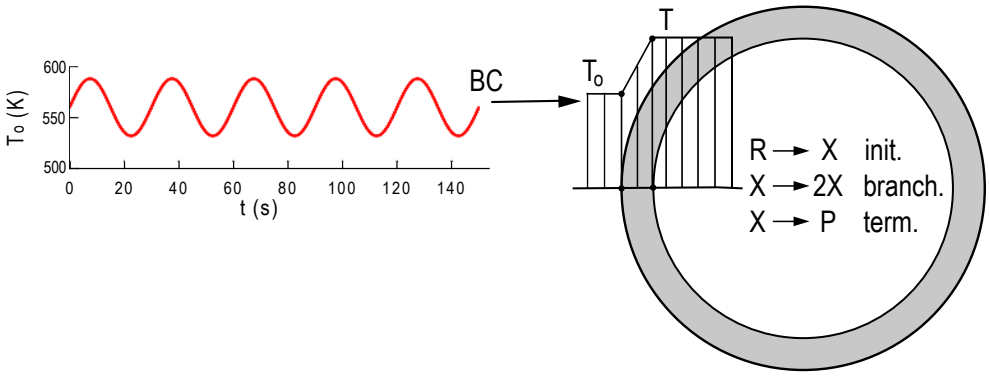

Figure 2.6: A simple diagram for how forcing is being implemented on the boundary condition temperature T_0 (on the *outside* of the combustion chamber).

The dynamical system as a whole is changed from non-autonomous to autonomous, introducing time as a third variable and essentially changing the state space from 2-dimensional to 3-dimensional (with one axis being time). The energy equation then takes the form:

$$\frac{dT}{dt} = \frac{1}{c_v}\Big(k_i h_i + (k_{t1}h_{t1} + k_{t2}h_{t2} + k_b h_b)X - \frac{\Gamma\lambda}{d^2}(T - \bar{T_0}(1 + A\sin(2\pi f t))\,)\Big) \tag{2.8}$$

Where A is the oscillation amplitude and f is the forcing frequency, which must be slower than the natural frequency of the system. T_0 is now denoted by $\bar{T_0}$, the average outer wall temperature. The oscillation amplitude can be no greater than about 5% in this system, because if it is greater the system blows up mathematically through unbounded exponential growth (this corresponds to the system exceeding the explosion limits determined by Yang & Gray). Taking the maximum possible amplitude of 5% (to obtain the strongest effect on the system), and taking f to be 1/60 Hz ($\tau = 60s$), the system exhibits periodic pulsation, as seen in Figure 2.7.

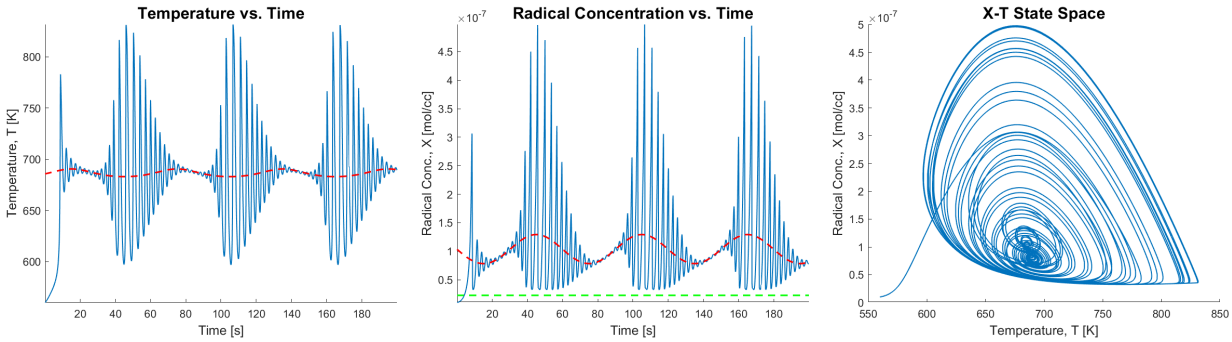

(a) Temp response (b) Radical Conc. response (c) X-T State Space.

Figure 2.7: Attractor behavior with periodic T_0

The red dashed line on each graph in Figure 2.7 again represents the second fixed point of the system, which from here on will be referred to as the central fixed point. As seen in Figures 2.7a and 2.7b, introducing an oscillation on the control parameter induces an oscillation of the same forcing frequency on the value of the central fixed point. More importantly, however, is the fact that the characteristic values now oscillate as well, and in such a way that the real part of the complex-conjugate pair of characteristic values periodically changes sign, as seen in the middle plot of Figure 2.8.

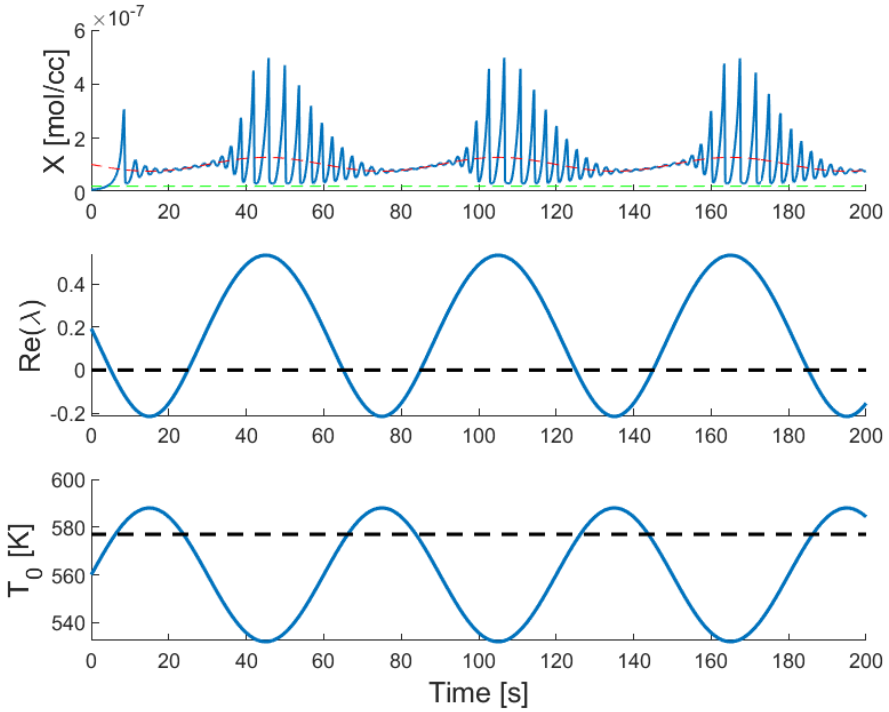

Figure 2.8: Temperature, Re(λ), and T_0 versus Time.

The real part of the characteristic values changes sign whenever T_0 crosses the Hopf bifurcation point at 578K. Every time that this change in sign occurs, the central fixed point changes between a spiral node and a spiral repellor (paired with the limit cycle). Based on this observation (and exploration of the values for A and f), it appears that there are just two criteria for a nonlinear dynamical system to exhibit periodic pulsation:

1. The system must exhibit a Hopf Bifurcation for some range of control parameter values.

2. There must be some periodic forcing on the control parameter, with a frequency lower than that of the natural frequency of the system.

The evolution of the periodic pulsation pattern as f is varied is given in Fig. 2.9, and shows that for very low forcing frequencies the oscillations of the system appear to die out completely (or "flat-line"). It should be noted that the fast frequency/timescale of the system is still governed by the chemical kinetics of the Semenov branching.

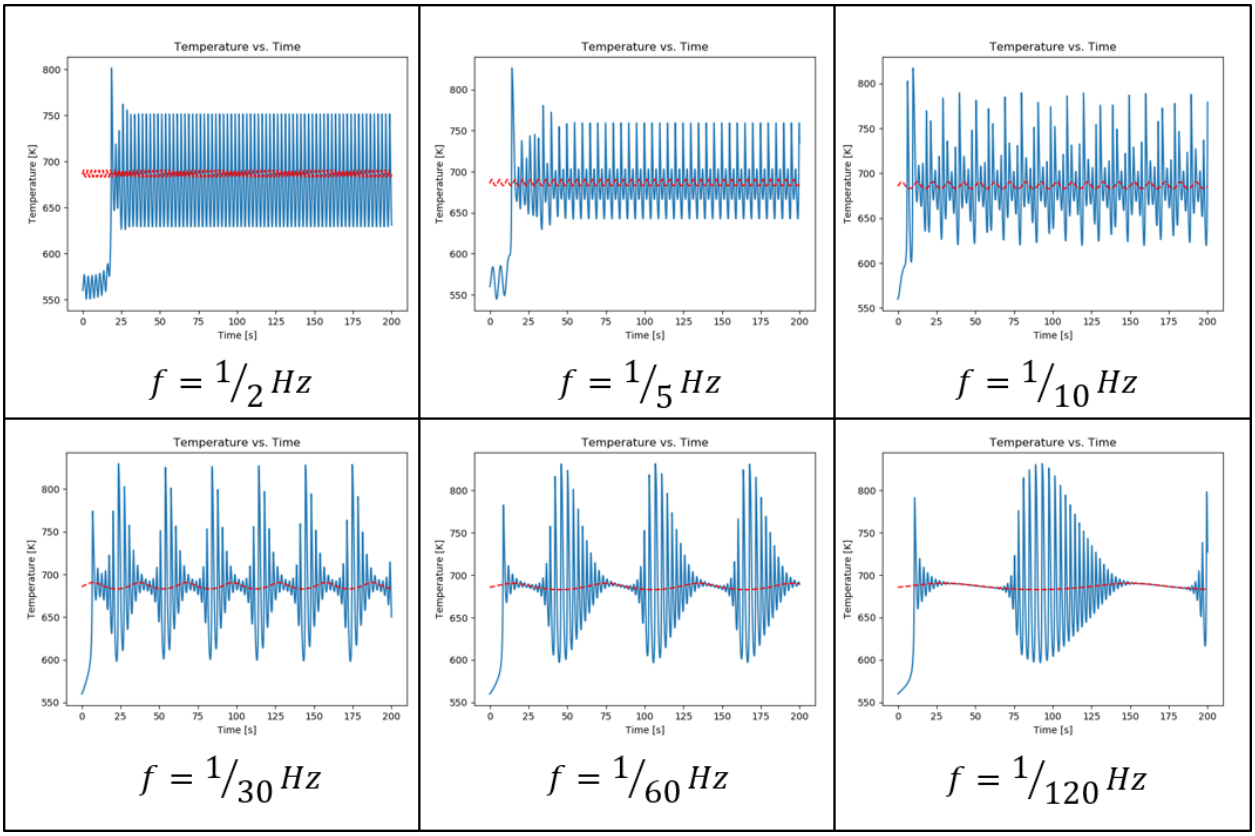

Figure 2.9: $A = 0.05$, $\bar{T}_0 = 560K$. The evolution of the periodic pulsation pattern as the slow forcing frequency decreases.

When the system exhibits periodic pulsation behavior, the assymetry in each pulse is due to the trajectory's detachment from the limit cycle. When the attractor switches from the limit cycle to the spiral node (at the trailing end of each pulse), the trajectory is no longer bound to the limit cycle and is exponentially drawn towards the spiral node. This transition appears fairly smooth because the limit cycle gradually becomes very small as the trajectory approaches the bifurcation point from the limit cycle side. On the other hand, when the attractor switches from the spiral node to the spiral repellor/limit cycle (at the leading end of each pulse), it takes more time for the trajectory to exponentially move away from the spiral repellor than it takes for the limit cycle to grow. Essentially the spiral node had pulled the trajectory in so close to itself, that once the limit cycle reappears, the trajectory needs more time to "climb" back up and reattach to the limit cycle. This idea of detachment is more readily apparent for what can be called "strong" periodic

pulsation, where $f_n >> f$ (f_n is the natural frequency in Hz).

Now, looking at the parametric curves of the characteristic values in the complex plane in Fig. 2.10, again it can be seen that the real part of the characteristic values lies on both sides of the imaginary axis (both positive and negative real values). The length of the curve on each side of the imaginary axis corresponds to the relative amount of time that each of the attractors exists in one period of the slow forcing frequency. As seen in Fig. 2.10, the portion of the curves to the right of the imaginary axis is greater than that to the left; therefore the characteristic values spend more time in one period with their real parts positive rather than negative, and hence the limit cycle exists for a larger portion of time in one period than does the spiral node.

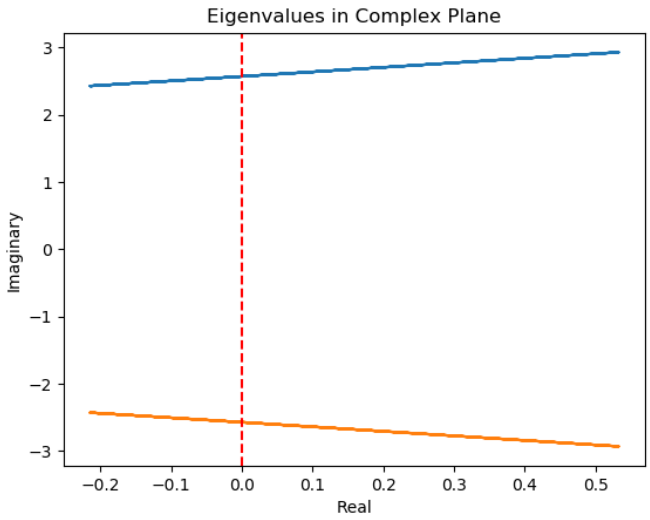

Figure 2.10: A=0.05, $\bar{T}_0$=560K. Characteristic values of the central fixed point in the complex plane. The curves are parametric in time, tracing out the paths taken in one period of the forcing frequency.

In order to provide a stronger basis for the two criteria for periodic pulsation outlined earlier, it is necessary to take those requirements and produce the same pulsation behavior in other nonlinear dynamical systems. Chapters 3 & 4 will discuss the second and third models mentioned in the introduction: the Simple Hopf Bifurcation model, and the Van der Pol oscillator.

CHAPTER 3

CFD SIMULATIONS

One of the other goals of this research was to try to model the pulsation seen in the Hong *et al.* experiment [1] through computational fluid dynamics (CFD) simulation. The time-varying nature of the pulsation required that the simulation be fully transient, but a sort of 'saving grace' in terms of dimensionality was the fact that the experiment used a cylindrical combustion chamber with an annular injector. This implies that we can apply an axisymmetric assumption to reduce the dimensionality from (3D+time) to (2D+time). Our initial computations use a relatively simple combustion mechanism for methane in order to gain some insight into producing periodic pulsation in our simulations. So far we have been able to generate only a single pulse (likely due only to transients in the solution steps), but even this gives us valuable information as we proceed to more complex chemical mechanisms.

3.1 Simulation Setup

Some preliminary work has been done in an attempt to reproduce periodic pulsation in a swirl combustor in CFD using ANSYS Fluent. The simulation is fully transient, and uses quasi-3-dimensional axisymmetric swirl geometry. A realizable k-ϵ model is used for turbulence calculations; while Large Eddy Simulation (LES) is more accurate and has already been used by others in similar geometries [19], the k-ϵ model is sufficient for our purposes in producing a ring vortex associated with backward-step injector geometries. It should be noted that the ring vortex (recirculation "bubble") is not really captured well by k-ϵ, but we are more concerned about the concept than the accuracy of its position and size. For combustion modeling, the simulation uses species transport governed by the four-step Jones and Lindstedt mechanism for the oxidation of methane [20], which has been used previously in the simulation of internal reacting flow of supersonic burners [21]. The eddy dissipation concept (or EDC) is used to model the turbulence-chemistry interaction. Although methane does not exhibit intermediate temperature cool-flame behavior like

some of the higher hydrocarbons (such as propane), the four-step reaction serves as a good starting point for the investigation of how periodic pulsation could develop in a lean-premixed swirl combustor. Current work is examining the minimum set of reduced chemistry that can lead to periodic pulsation in the CFD system.

The combustor geometry is taken to match the dimensions used in the Hong *et al.* experiment [1]. The combustion chamber has a length of 700mm and a vessel radius of 40mm, and the annular injector has an outer radius of 14mm and an inner radius of 11mm. We used a rectangular element mesh of 64,120 cells, with higher cell density near the injector where combustion takes place (part of our current work is concerned with mesh sizing and convergence studies). In the simulations, we started with a stoichiometric premixed mixture ($\phi = 1$) of methane and air injected into the combustion chamber just before the backward-facing step (the injector face). The combustion chamber is allowed to reach species equilibrium, and the mixture is ignited using a brief heat source (using a "spark" in the simulation) just above the injector face along the central axis of the chamber.

3.2 Chemical Kinetics

The Jones and Lindstedt [20] is a four-step mechanism that involves only major species for methane oxidation:

$$R1: \quad \mathrm{CH_4} + \frac{1}{2}\mathrm{O_2} \rightarrow \mathrm{CO} + 2\mathrm{H_2} \tag{3.1}$$

$$R2: \quad \mathrm{CH_4} + \mathrm{H_2O} \rightarrow \mathrm{CO} + 3\mathrm{H_2} \tag{3.2}$$

$$R3: \quad \mathrm{CO} + \mathrm{H_2O} \leftrightharpoons \mathrm{CO_2} + \mathrm{H_2} \tag{3.3}$$

$$R4: \quad \mathrm{H_2} + \frac{1}{2}\mathrm{O_2} \leftrightharpoons \mathrm{H_2O} \tag{3.4}$$

Two different fuel oxidation paths are used to make the mechanism applicable to both premixed and non-premixed flames. The water gas shift reaction (R3), which is important in the determination of flame structure for all HC flames, is included in this mechanism. The low computational expense along with the availability of kinetic rate data for the reduced reaction set made

this a suitable mechanism for finite-rate calculations in our (2D+time) computations. The reaction parameters are shown in Table 3.1.

Table 3.1: Kinetic Rate data of the Jones and Lindstedt mechanism. Concentrations, denoted by square brackets, are in units of kmol/m^3. All Arrhenius parameters have zero temperature exponent.

No.	A (kmol/m$^3 s$)	E_a/R (K)	Reaction orders
R_1	4.40×10^{11}	15,095	$[CH_4]^{0.5}[O_2]^{1.25}$
R_2	3.00×10^{8}	15,095	$[CH_4][O_2]$
R_{3f}	2.75×10^{9}	10,065	$[CO][H_2O]$
R_{3b}	6.71×10^{10}	13,688	$[CO_2][H_2]$
R_{4f}	5.69×10^{11}	17,609	$[H2][O_2]^{0.5}$
R_{4b}	2.51×10^{14}	47,859	$[H_2O]$

These Arrhenius parameters and reactions are input into the simulation manually (i.e. Fluent does not read an external kinetics/reactions file), and thermodynamic data for each species in the mechanism is taken from Fluent's thermodynamic database.

3.3 Preliminary Results

In both the steady-state and transient solutions, we were able to generate flame holding at the central face of the annular injector. An example of this is given in Fig. 3.1 below – the steady state solution – which helped to verify that the chemical mechanism and thermodynamics were being computed properly before we moved on to the fully transient simulations. In this steady state solution with stoichiometric reactants, we achieved a flame temperature of 2207K; for reference, the literature value for the adiabatic flame temperature of a stoichiometric mixture of methane and air is 2226K [18] – a discrepancy of 0.9% (the difference is likely due to heat loss at the boundaries

of the combustion chamber). Fig. 3.1 also shows the velocity streamlines for the steady state solution, and we can see that the outer ring vortex is clearly defined.

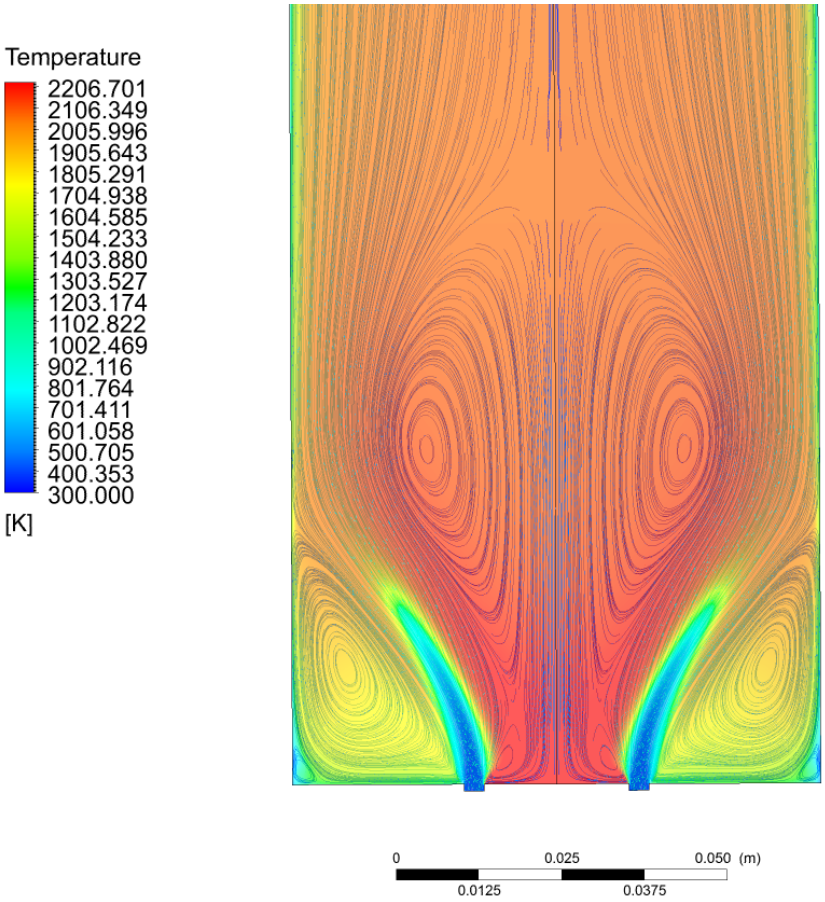

Figure 3.1: Steady-state combustion solution using the Jones & Lindstedt mechanism for methane combustion. Temperature in the combustion chamber is plotted as the color contour, and velocity streamlines are overlayed. Only the portion of the simulation near to the injector is shown.

An example of the transient solution flame is given below in Fig. 3.2. If the transient simulation is run for many time steps (a long simulation time, likely on the order of 1 minute), the high temperature region proceeds up the combustion chamber and the solution approaches the steady state solution of Fig. 3.1.

Out of all of our transient simulations, we have only been able to produce a pressure pulse once.

The pressure trace of the pulse is given in Fig. 3.3; the values of which were taken at the point marked by the yellow dot on the combustion chamber axis shown in Fig. 3.2. Time snapshots of the simulation during the pulse are given in Figs. 3.4 & 3.5. The time step used for the simulation was 0.01sec, with ignition beginning at 0.05sec (again, with a heat source just above the injector face along the central axis).

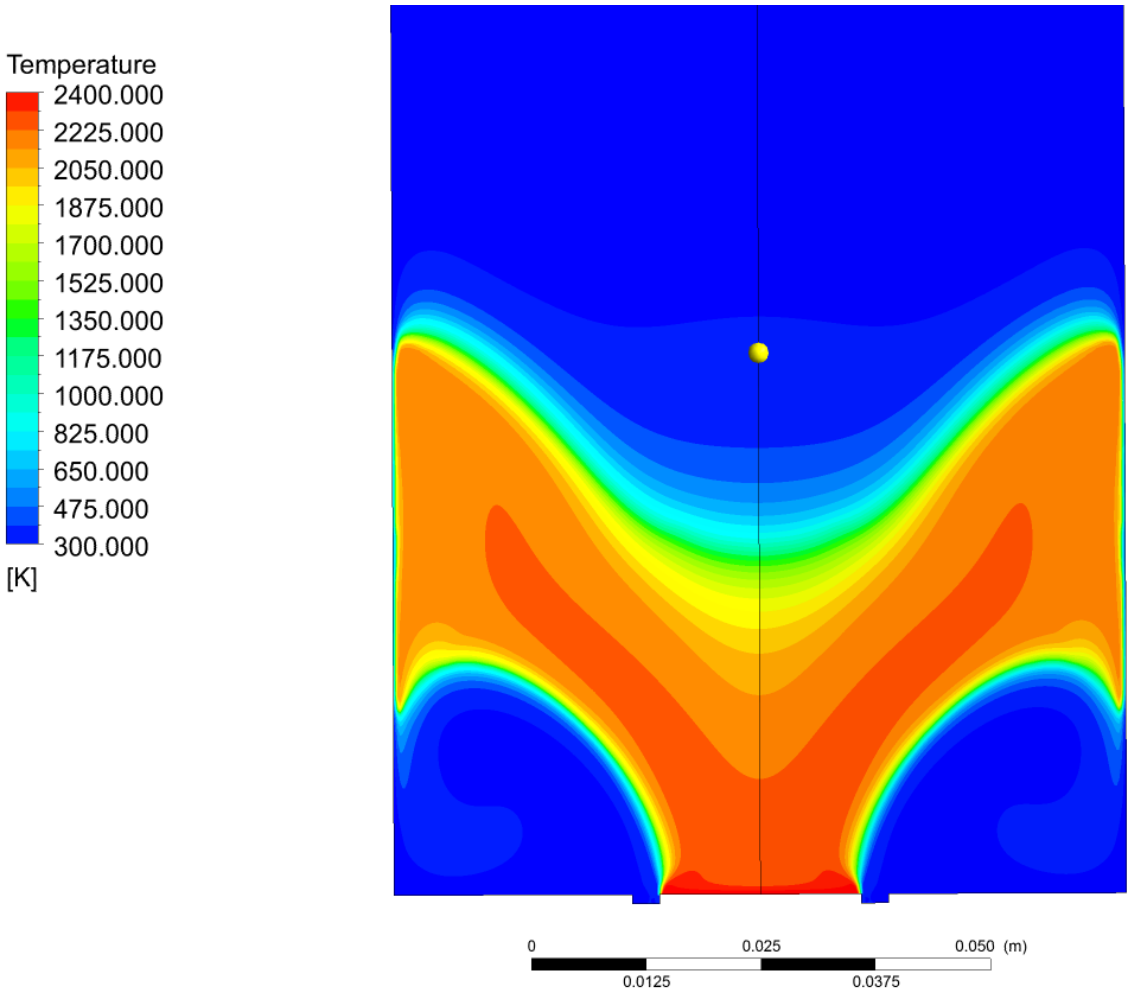

Figure 3.2: An example flame at a single time step of the transient combustion simulation.

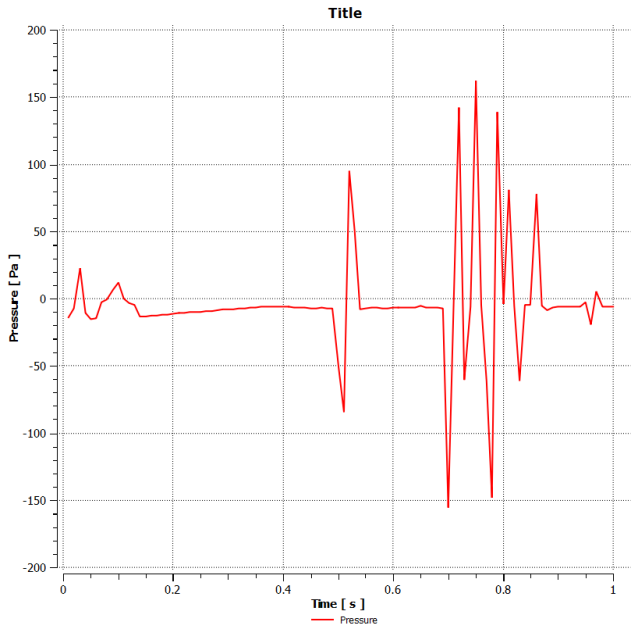

Figure 3.3: A single transient pressure pulse generated in one of the combustion simulations. Pressure values on the y-axis are gauge pressure.

After this pulse, we continued the simulation for an additional second of simulation time; however, no additional pulses were seen. It should be noted that this particular simulation was run with stoichiometric (not lean) reactants. We have not yet determined what exactly caused the pulse, but we postulate that heat loss could still be the culprit for periodic pulsation – as it is for the reduced order Combustion model. The "pulse" we see here is most likely an artifact of the code transient behavior, and not physical.

In all of the snapshots of Fig. 3.4, a low pressure area in the lower left corner can be seen; this area corresponds to the outer ring vortex generated due to the backward-facing-step of the injector port. One interesting observation is that if we look at the same time step in both Fig. 3.4 and Fig. 3.5, we see that spikes of low pressure in the combustion chamber correspond to higher average temperatures within the flame region, and vice versa. This is in contrast with the intuitive expectation that higher pressures should correspond to higher temperatures, and is another reason we believe the pulse we see here is not physical.

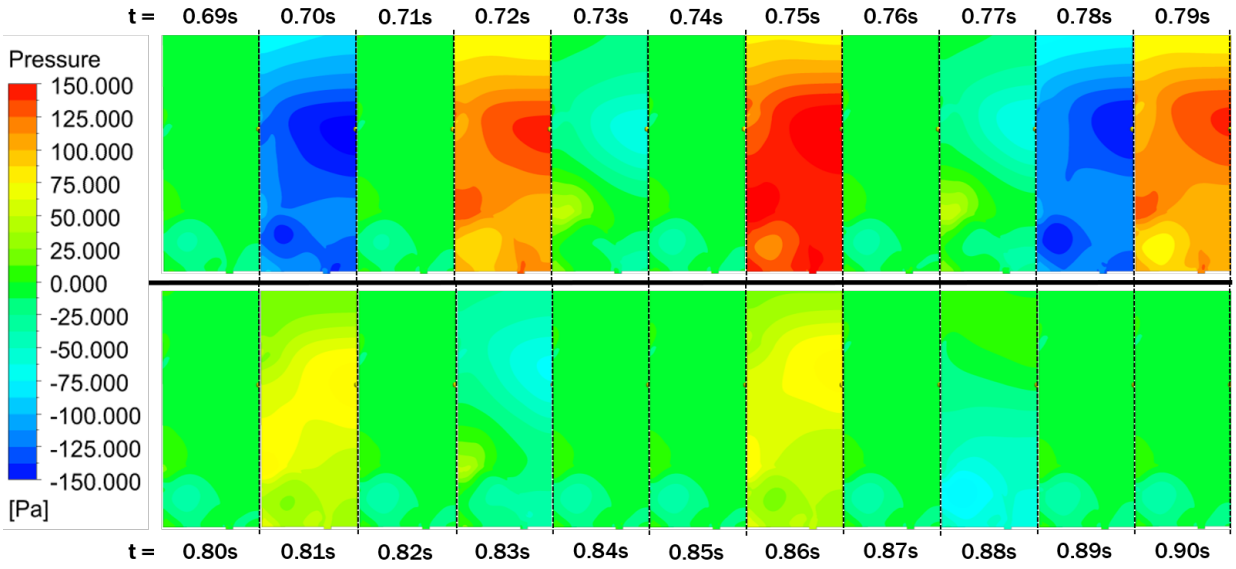

Figure 3.4: A series of *gauge* pressure snapshots of the combustion simulation during the pressure pulse seen in Fig. 3.3 above. Only half of the combustion chamber is displayed in each snapshot, with the black dashed line representing the central axis (on the right side of each snapshot).

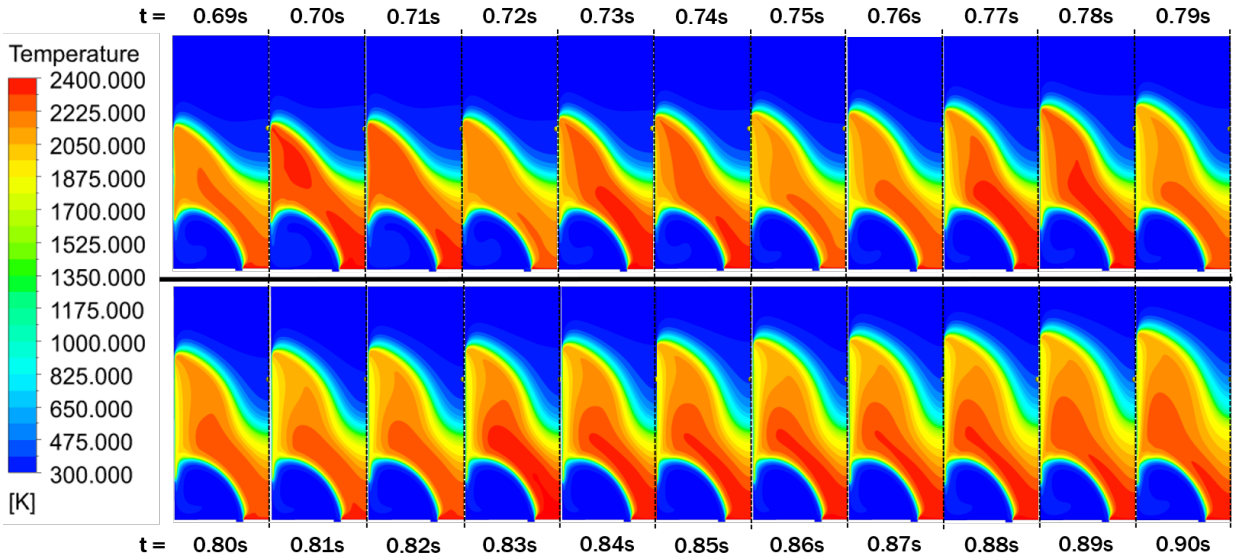

Figure 3.5: A series of temperature snapshots of the combustion simulation during the pressure pulse seen in Fig. 3.3 above. Only half of the combustion chamber is displayed in each snapshot, with the black dashed line representing the central axis (on the right side of each snapshot).

Current work studies both lean-burning conditions, following the successful stoichiometric simulation, as well as slightly more complex chemical mechanisms for propane instead of methane. We will attempt to create a reduced chemical mechanism for propane for two reasons: a) propane (LPG) was the main component of the fuel in the experiment by Hong *et al.* [1]; and, b) propane can exhibit oscillatory cool-flame phenomena at lean burning conditions, which we believe is related to the slow forcing mode for periodic pulsation through its effects on heat loss.

CHAPTER 4

THE SIMPLE HOPF BIFURCATION MODEL

The two criteria for periodic pulsation outlined in Section 1.4 led us to search first for systems that had a Hopf bifurcation. The first (and simplest) one was found in Hilborn's text on nonlinear dynamics and chaos [10]. We will refer to the system as the Simple Hopf Bifurcation (SHB) model. Applying the second criterion, periodic pulsation can be produced in the SHB. In fact, the SHB can exhibit more rich dynamical behavior than the Combustion model – an example of which is best described as an "arrhythmia" bifurcation. This particular system was simply meant to model a limit cycle/ Hopf bifurcation, and as such it does not necessarily have a direct physical analogue.

4.1 Periodic Pulsation in the Simple Hopf Bifurcation

The basic system of equations for the SHB model is as follows:

$$\vec{f}(x_1, x_2) = \begin{cases} f_1 = \dot{x_1} = -\omega_n x_2 + x_1\big(\mu - (x_1^2 + x_2^2)\big) \\ f_2 = \dot{x_2} = \omega_n x_1 + x_2\big(\mu - (x_1^2 + x_2^2)\big) \end{cases} \tag{4.1}$$

Where μ is the control parameter (which affects damping in the system). As Hilborn explained, it is convenient to transform this particular system into polar coordinates (r,θ) with the origin at $(x_1, x_2) = (0, 0)$. The new system of equations, as well as its Jacobian matrix, then become:

$$\vec{f}(r, \theta) = \begin{cases} f_1 = \dot{r} = r(\mu - r^2) \\ f_2 = \dot{\theta} = \omega_n \end{cases} \tag{4.2}$$

$$[J] = \begin{bmatrix} \mu - 3r^2 & 0 \\ 0 & 0 \end{bmatrix} \tag{4.3}$$

For $\mu < 0$, the system has one spiral node fixed point at $r^* = 0$, or $(x_1, x_2) = (0, 0)$. For $\mu > 0$,

the system has a spiral repellor fixed point again at $r^* = 0$, but an additional fixed point at $r = \sqrt{\mu}$, corresponding to a limit cycle. Therefore the Hopf bifurcation point (where the limit cycle is born) is at $\mu = 0$. Taking $|\mu| = 0.05$, the state space for each attractor can be seen in Figure 4.1

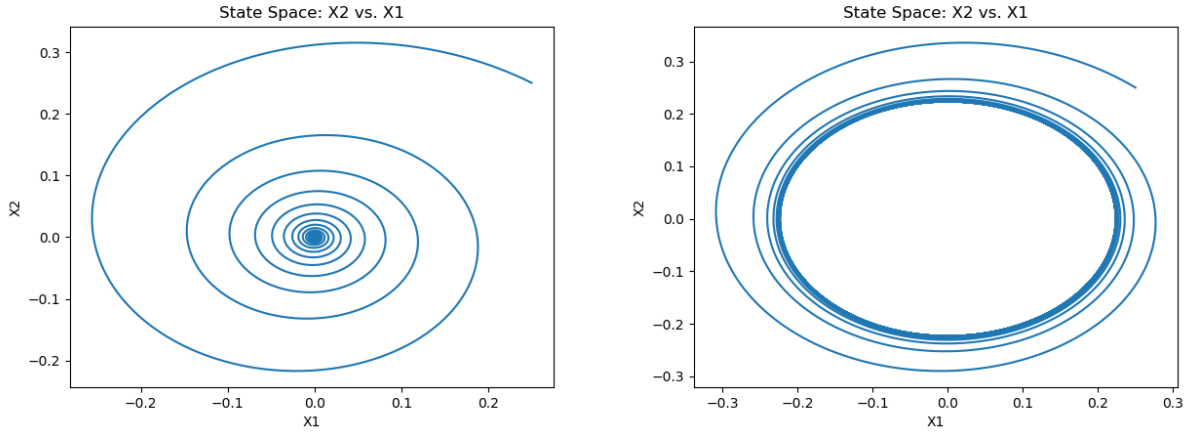

(a) $\mu = -0.05$ (b) $\mu = +0.05$

Figure 4.1: x_1, x_2 state spaces in the unforced SHB.

If forcing is now added to the control parameter in the $\dot{x_1}$ equation of Eqn. 4.1, the original system becomes:

$$\vec{f}(x_1, x_2) = \begin{cases} f_1 = \dot{x_1} = -\omega_n x_2 + x_1\big(\mu' - (x_1^2 + x_2^2)\big) \\ f_2 = \dot{x_2} = \omega_n x_1 + x_2\big(\bar{\mu} - (x_1^2 + x_2^2)\big) \end{cases} \quad , \quad \mu' = \bar{\mu}\big(1 + A\sin(\frac{2\pi}{\tau}t)\big) \tag{4.4}$$

It should be noted that the μ value in the $\dot{x_2}$ equation could instead have been forced. What really matters is that only *one* of the original $\dot{x_1}$ or $\dot{x_2}$ equations contains the forcing term. Further study is required to explore the case when μ is forced in both equations (as it would be more correct to do so according to the unforced polar system of Eqn. 4.2). For now, the parameter $\bar{\mu}$ in each of the two equations can be thought of as separate parameters with the same numerical value.

Again, this system has a fixed point at $(x_1, x_2) = (0, 0)$, and just like in the analysis of the

second fixed point of the combustion model, this is the central fixed point that generates periodic pulsation behavior in the SHB. Using $\bar{\mu} = 0.05$ and $A = 10$, Figure 4.2 shows the evolution of the system response as the forcing period increases (note: the system has a natural radial frequency of 1 rad/s):

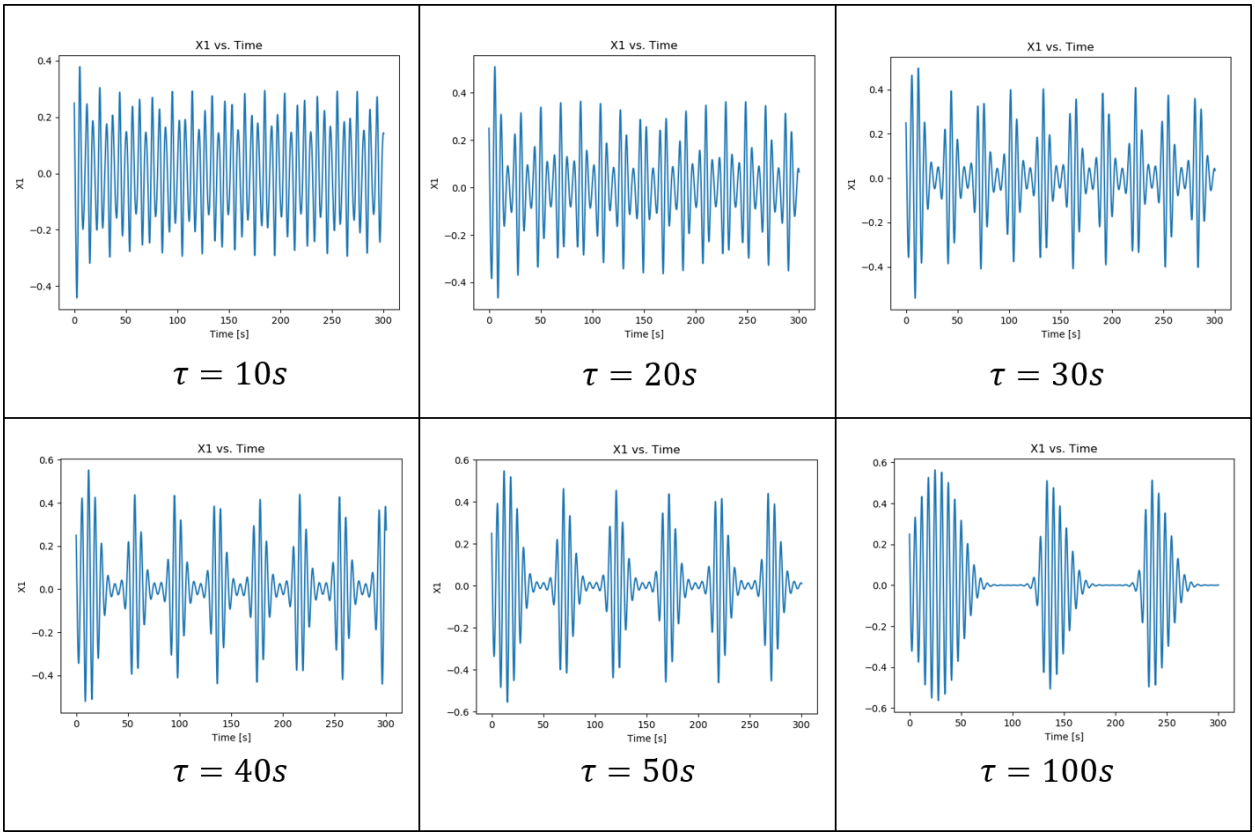

Figure 4.2: $A = 10$, $\bar{\mu} = 0.05$, $\omega_n = 1$. Evolution of the periodic pulsation pattern in the SHB as the slow forcing period increases (forcing frequency decreases).

Now looking at the behavior of the control parameter, the real part of the characteristic values of the central fixed point, and the system response in Figure 4.3, it can again be seen that whenever the control parameter crosses the bifurcation point at $\mu = 0$, the real part of the characteristic values changes sign and the attractor switches between the spiral node and the limit cycle.

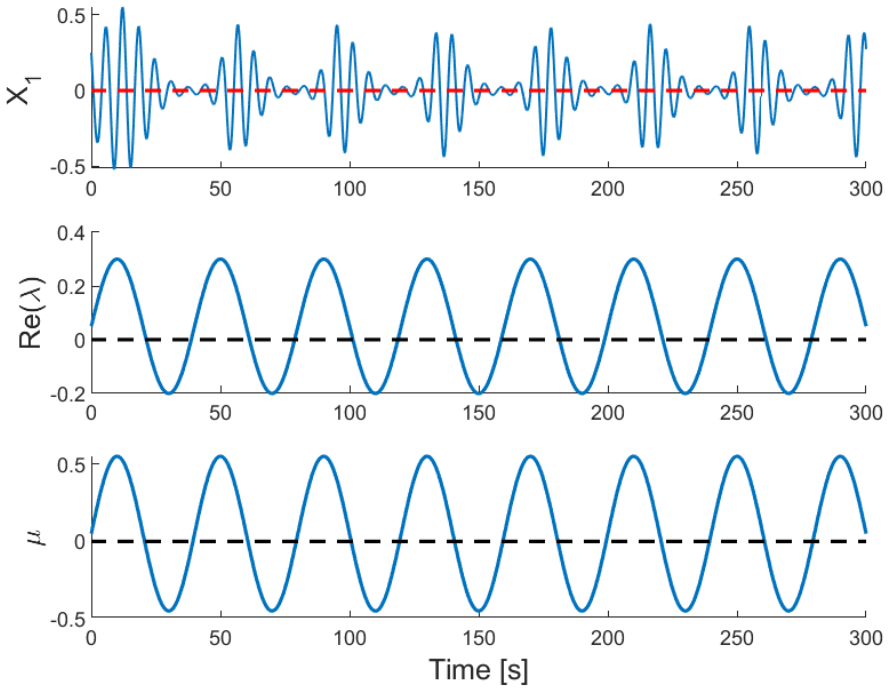

Figure 4.3: x_1, Re(λ), and μ versus Time. $A = 10$, $\bar{\mu} = 0.05$, $\omega_n = 1$.

One noticeable difference between the SHB model and the Combustion model discussed in the previous section is the behavior of the characteristic values in the complex plane.

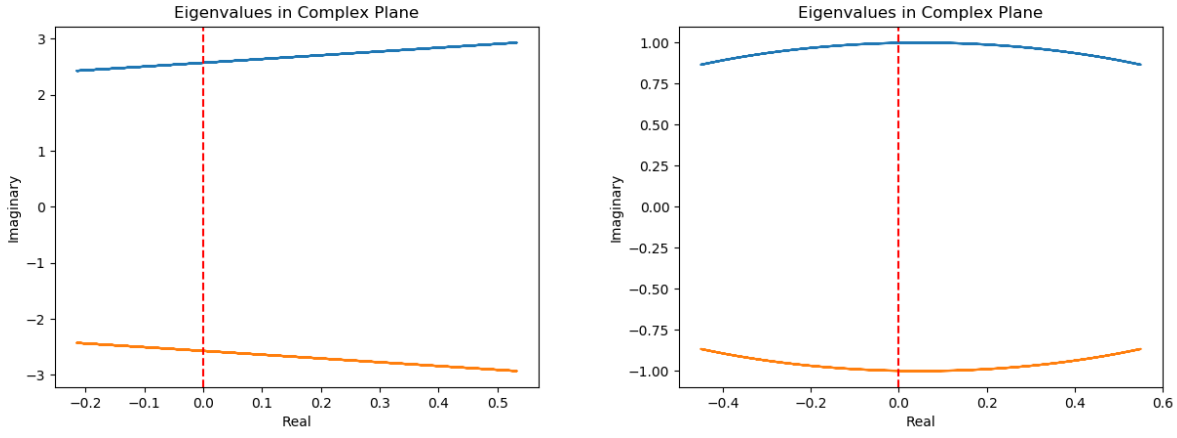

(a) Combustion model: $A = 0.05$, $\bar{T}_0 = 560$

(b) SHB model: $A = 20$, $\bar{\mu} = 0.05$, $\omega_n = 1$

Figure 4.4: Model comparison: Characteristic values in the complex plane.

The characteristic values of the Combustion model move along straight lines in the complex plane, whereas the characteristic values of the SHB model move along the perimeter of a circle that is shifted to the right or left of the imaginary axis by the value $\bar{\mu}$. The amplitude of the oscillations for the SHB was increased to 20 in Figure 4.4b in order to accentuate the curvature. In fact if the the amplitude is increased further, the characteristic values complete the circle, as seen in 4.5a. For $\bar{\mu} = 0.05$, this occurs exactly when $A = 40$ as we shall see later. If the amplitude is increased further still – larger than a value of 40 – then the complex conjugate pair of characteristic values that were previously on the circle become a pair of real characteristic values. Figure 4.5b shows a case where $A > 40$.

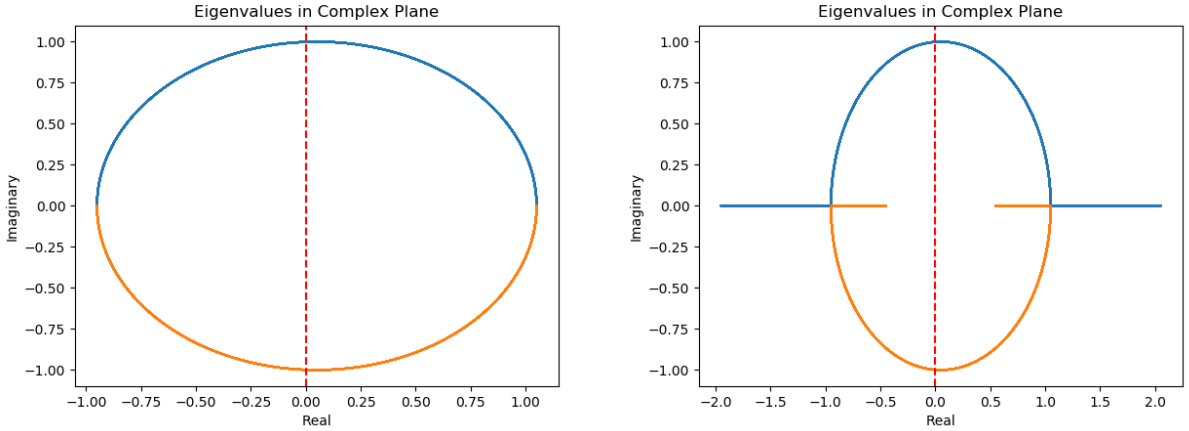

(a) $A = 40$ (b) $A = 50$

Figure 4.5: Characteristic values comparison in complex plane. $\tau = 50s$, $\bar{\mu} = 0.05$, $\omega_n = 1$.

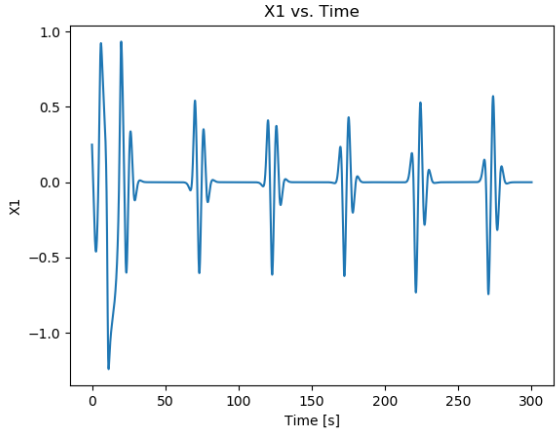

(a) $A = 40$

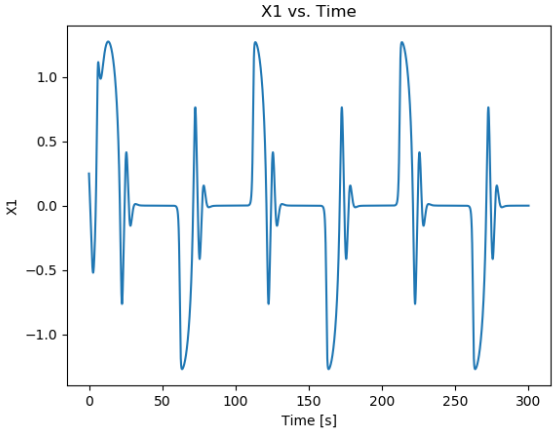

(b) $A = 50$

Figure 4.6: System response comparison. $\tau = 50s$, $\bar{\mu} = 0.05$, $\omega_n = 1$.

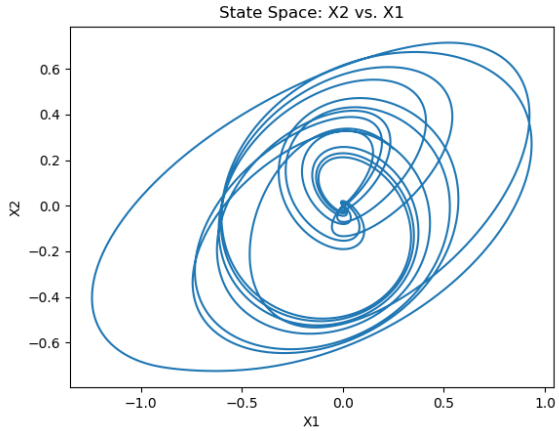

(a) $A = 40$

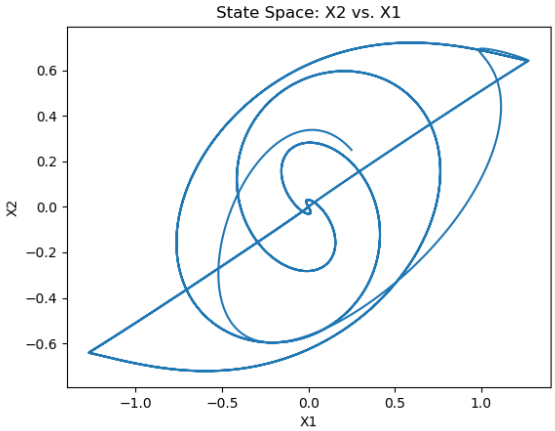

(b) $A = 50$

Figure 4.7: State space comparison. $\tau = 50s$, $\bar{\mu} = 0.05$, $\omega_n = 1$.

In Figure 4.6a, something resembling a heartbeat pattern has emerged after transients have dissipated. Essentially the amplitude has increased to the point where the spiral node pulls on the trajectory a great deal and a large amount of detachment occurs when the limit cycle reappears. The detachment is so large that once the trajectory actually reattaches (if at all) to the limit cycle, too much time has passed and the spiral node appears again. In Figure 4.6b, the amplitude has been increased beyond the critical value of 40 and the characteristic values periodically become real with opposite sign twice in every forcing period. The effect of this change in the nature of the characteristic values on the system response is best described as an "arrhythmia", based on a visual inspection of the response (either X_1 or X_2) and a comparison to heartbeat nomenclature. The reasons for $A = 40$ being the critical value for the arrhythmia to appear when $\bar{\mu} = 0.05$, as well as the intervals and times in each forcing period at which they occur, will now be discussed.

4.2 Arrhythmias in the Simple Hopf Bifurcation

Deriving the time intervals when arrhythmias appear/disappear begins with determining the central fixed point of the system by setting our equations equal to 0:

$$\begin{cases} \dot{x_1} = -\omega_n x_2 + x_1\big(\bar{\mu}(1 + AB) - (x_1^2 + x_2^2)\big) = 0 \\ \dot{x_2} = \omega_n x_1 + x_2\big(\bar{\mu} - (x_1^2 + x_2^2)\big) = 0 \end{cases} , \qquad B = \sin\Big(\frac{2\pi}{\tau}t\Big) \tag{4.5}$$

A is the forcing amplitude, and we define B simply for the sake of brevity. Again, τ is the period of the slow forcing mode. For this system of equations, the central fixed point is (x_1^*, x_2^*) = (0, 0). The characteristic values of this fixed point (λ) are determined by evaluating the determinant of the Jacobian at the fixed point and setting it equal to 0 (i.e. finding the eigenvalues of the Jacobian at the fixed point):

$$\det[J|_* - \lambda I] = \det \begin{bmatrix} \bar{\mu}(1 + AB) - \lambda & -\omega_n \\ \omega_n & \bar{\mu} - \lambda \end{bmatrix} = 0 \tag{4.6}$$

which yields the characteristic equation for the system:

$$\lambda^2 - \bar{\mu}\lambda(2 + AB) + (\omega_n^2 + \bar{\mu}^2(1 + AB)) = 0 \tag{4.7}$$

Through the quadratic formula, we have the function for how the characteristic values of the fixed point change with time:

$$\lambda_{1,2} = \frac{\bar{\mu}}{2}(2 + AB) \pm \frac{1}{2}\sqrt{\bar{\mu}^2 A^2 B^2 - 4\omega_n^2} \tag{4.8}$$

Normally, the argument of the square root in Eqn. 4.8 is less than 0, meaning the characteristic values form a complex-conjugate pair. However, under the correct set of parameters, the argument of the square root can be positive – making the characteristic values a pair of real numbers. When this occurs, the system exhibits an arrhythmia. In short, an arrhythmia exists when:

$$\bar{\mu}^2 A^2 B^2 - 4\omega_n^2 \geq 0 \tag{4.9}$$

Rearranging the above inequality yields:

$$0 \leq \left| \frac{2\omega_n}{\bar{\mu}AB} \right| \leq 1 \tag{4.10}$$

However, a more useful form of the above inequality for determining the times for arrhythmias moving forward is:

$$|B| = \left| \sin\left(\frac{2\pi}{\tau}t\right) \right| \geq \left| \frac{2\omega_n}{\bar{\mu}A} \right| \geq 0 \tag{4.11}$$

Which cannot be satisfied for $B = 0$ (for $A > 0$ and $\bar{\mu} > 0$), which occurs at times $t = 0,\ \frac{n\tau}{2}\ \ (n = 1, 2, 3, ...)$. More generally, the inequality cannot be satisfied if B is "near enough" to 0, with "near enough" being defined by the value $|\frac{2\omega_n}{\bar{\mu}A}|$. In other words, the characteristic values will be real in the time intervals where $|B|$ is greater than this value. It is fairly straightforward to

determine these time intervals. Rearranging Eqn. 4.11, we define a time, t_0, as follows:

$$t_0 = \frac{\tau}{2\pi} \sin^{-1}\left(\left|\frac{2\omega_n}{\bar{\mu}A}\right|\right) \tag{4.12}$$

which is real only when:

$$0 \leq \left|\frac{2\omega_n}{\bar{\mu}A}\right| \leq 1 \tag{4.13}$$

or, for $A > 0$:

$$A \geq \left|\frac{2\omega_n}{\bar{\mu}}\right| \tag{4.14}$$

This gives us the critical value for A, or the bifurcation point for the arrhythmia to appear. Looking at the previous cases where $\bar{\mu} = 0.05$ and $\omega_n = 1$, and inserting those values into Eqn. 4.14, we recover the previously stated critical value of $A = 40$. When Eqn. 4.14 is satisfied, the time t_0 is real and therefore intervals of time will exist in each forcing period where the characteristic values are real (i.e. the arrhythmia appears). For the sake of brevity we now define the constant angle ϕ as:

$$\phi = \sin^{-1}\left(\left|\frac{2\omega_n}{\bar{\mu}A}\right|\right) \tag{4.15}$$

which has the following two properties:

$$\lim_{A\to\infty} \phi = 0 \tag{4.16}$$

$$0 \leq \phi \leq \frac{\pi}{2} \tag{4.17}$$

Substituting this definition into Eqn. 4.12 we get:

$$t_0 = \frac{\tau}{2\pi}\phi \tag{4.18}$$

Now, from Eqn. 4.11, the characteristic values are real only when the following equation is satisfied:

$$|B| \geq \sin(\phi) = \left| \frac{2\omega_n}{\mu A} \right| = k \tag{4.19}$$

or more simply:

$$|B| \geq k \tag{4.20}$$

Here we have defined an "arrhythmia constant," k. The exact times at which $|B| = k$ correspond to the exact times when λ_1, λ_2 switch from a complex-conjugate pair to a pair of real values, and vice versa. Since $B = \sin(\frac{2\pi}{\tau}t)$, these discrete times allow us to write both the angular intervals and time intervals for which λ_1, λ_2 are real:

$$\begin{cases} \phi \leq \frac{2\pi}{\tau}t \leq \pi - \phi \\ \pi + \phi \leq \frac{2\pi}{\tau}t \leq 2\pi - \phi \end{cases} \tag{4.21}$$

$$\begin{cases} t_0 \leq t \leq \frac{\tau}{2} - t_0 \\ \frac{\tau}{2} + t_0 \leq t \leq \tau - t_0 \end{cases} \tag{4.22}$$

Another way to visualize this is to plot the angular intervals of Eqn. 4.21. The shaded regions in the figure below represent the angular intervals where λ_1, λ_2 are real, with the system angle (the argument of sine in B) rotating about the origin with a frequency of $2\pi/\tau$.

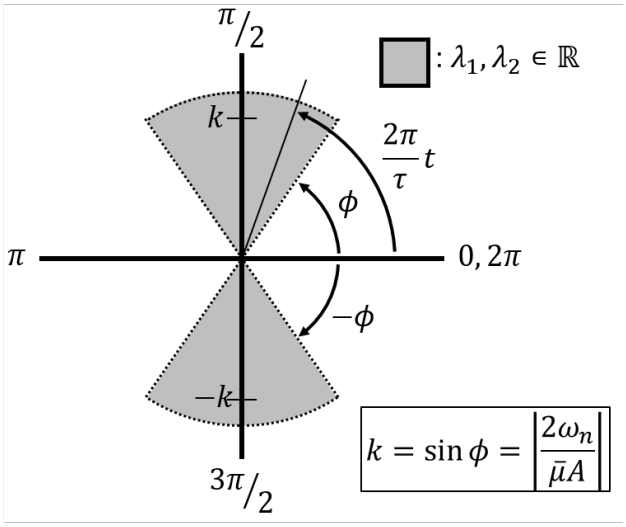

Figure 4.8: Visualization of the angular intervals where λ_1, λ_2 are real in the SHB.

While two arrhythmias must appear during each slow period according to Eqn. 4.22 and Fig. 4.8, only one arrhythmia is visually apparent in the system response at the beginning of each pulse. The reason for this is that while there are two arrhythmias per slow period, one appears during the limit cycle phase and the other appears during the spiral node phase. The arrhythmia that appears in the limit cycle phase is the one that appears at the beginning of each pulse. Looking at Fig. 4.9 below in the subplot for the real part of the characteristic values, we see that there are indeed two arrhythmias per forcing period; one during the limit cycle phase ($\mu > 0$) and one during the spiral node phase ($\mu < 0$). However, the limit cycle arrhythmia is much more apparent in the system response due to its drastically greater amplitude compared to the spiral node arrhythmia.

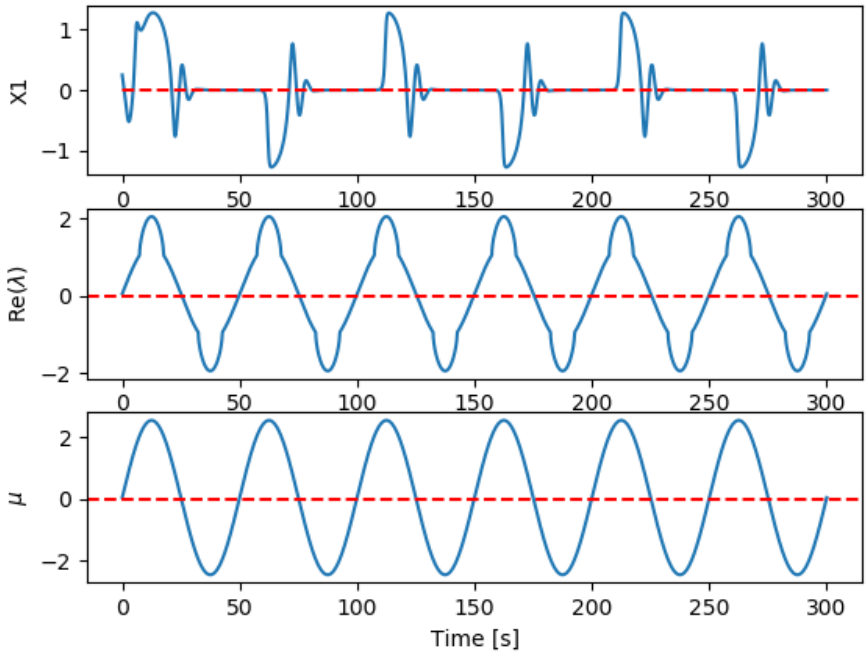

Figure 4.9: x_1, Re(λ), and μ versus Time. A=50, $\bar{\mu} = 0.05$, $\omega_n = 1$.

To summarize, arrhythmias in periodic pulsation are characterized by the periodic switching of the central fixed point's characteristic values from a complex-conjugate pair to a pair of real values. They will only appear in the SHB when the following two conditions are met (remembering that $B = \sin(\frac{2\pi}{\tau}t)$, and taking $A > 0$), and during the following time intervals, Δt:

$$\text{Cond.1)} \quad A \geq \left|\frac{2\omega_n}{\bar{\mu}}\right| \qquad\qquad \text{Cond.2)} \quad |B| \geq \left|\frac{2\omega_n}{\bar{\mu}A}\right| = k$$

$$\Delta t = \frac{\tau}{2} - 2t_0, \quad \& \quad t_0 = \frac{\tau}{2\pi}\sin^{-1}(k) \;\; ; \;\; \text{w/ intervals beginning at: } t = \frac{n\tau}{2} + t_0, \;\; n = 0, 1, 2, 3... \tag{4.23}$$

It is also possible to derive the arrhythmia equations above by converting the forced cartesian equations for ($\dot{x_1}$, $\dot{x_2}$) into polar equations for $(\dot{r}, \dot{\theta})$ and solving for the times when an "angular fixed point" appears and disappears. For the derivation of arrhythmia time intervals using the polar set of equations, see Appendix A.

CHAPTER 5

THE VAN DER POL OSCILLATOR

The Van der Pol Oscillator (VDP) is one of the most thoroughly studied relaxation oscillators, but instead of adding a forcing term to the end of the equations – as Van der Pol himself studied [11] – the forcing term is added to the control parameter (as with the previous models) and periodic pulsation is produced. We shall also see that the arrhythmia bifurcation described in the SHB model can also be produced in the Van der Pol oscillator – but with one slight difference.

One interesting note is that although the SHB did not have a direct physical representation, the VDP is based directly on an actual electrical circuit – implying that this circuit might be able to produce periodic pulsation in reality with the proper type of resistor.

5.1 Periodic Pulsation in the Van der Pol Oscillator

Referencing the Hilborn text, a modified form of the Van der Pol equation used is as follows (with the forcing term now added to the control parameter, R) [10]:

$$\vec{f}(x_1, x_2) = \begin{cases} f_1 = \dot{Q} = U \\ f_2 = \dot{U} = \Big(\bar{R}\big(1 + A\sin(\frac{2\pi}{\tau}t)\big) - Q^2\Big)U - \omega_n^2 Q \end{cases} \tag{5.1}$$

Where Q is the system charge and U is the current. R is the resistance/damping parameter of the circuit; it may be possible to have negative resistance in a physical version of the circuit (e.g. negative differential resistors), but it is unclear if forcing the resistance to periodically switch between positive and negative is possible in the physical circuit. Taking $A = 0$ (the unforced case), the system exhibits a Hopf Bifurcation when $R = 0$. The limit cycle exists when $R > 0$, and the spiral node exists for $R < 0$. Furthermore, if the periodic forcing is added back in (as in Eqn. 5.1), and setting $\bar{R} = 0.1$, $A = 10$, and $\omega_n = 1$, the effect of slowly increasing the forcing period τ can be seen in the Fig. 5.1.

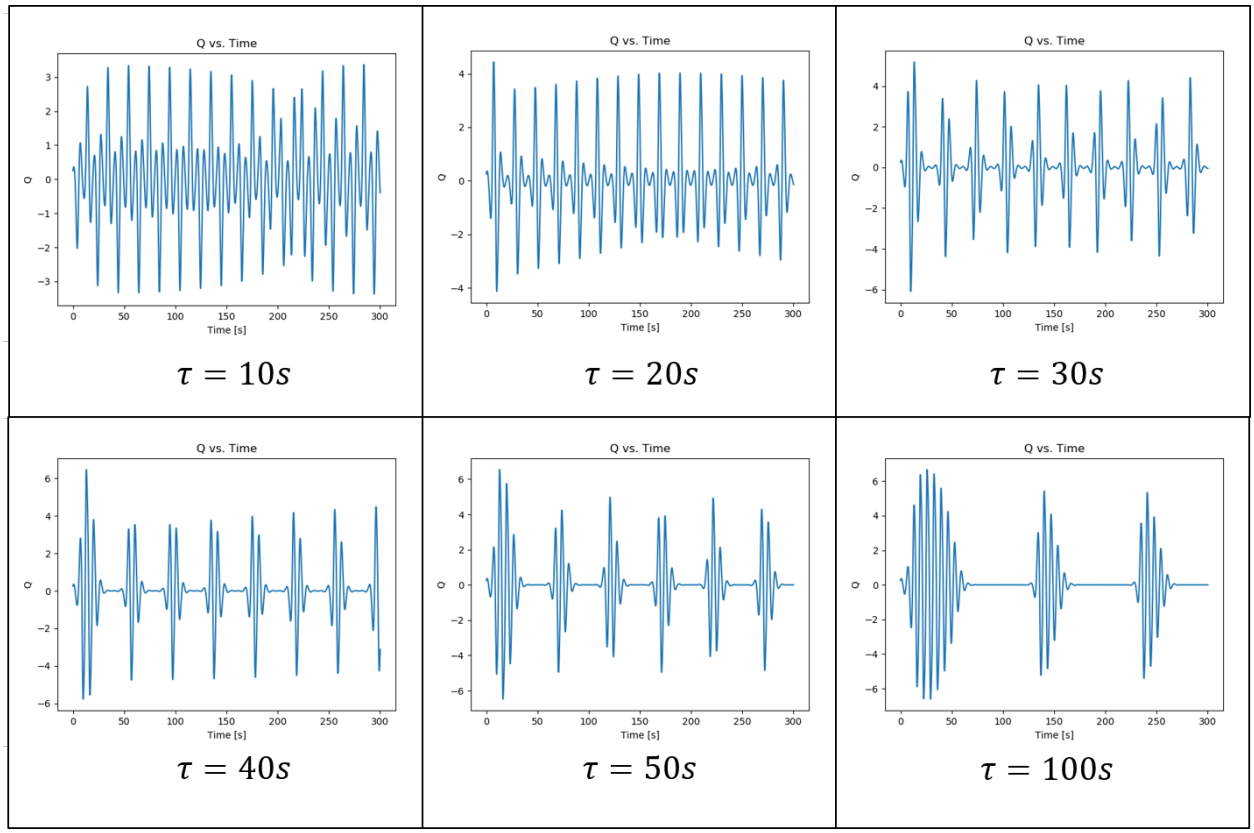

Figure 5.1: $A = 10$, $\bar{R} = 0.1$, $\omega_n = 1$. Evolution of the periodic pulsation pattern in the VDP as the slow forcing period increases (forcing frequency decreases).

The slow forcing mode is readily apparent when looking at the behavior of the characteristic values of the central fixed point and the control parameter R versus time. The periodic switching between the limit cycle and the spiral node and the effect on the system response can be seen in Fig. 5.2.

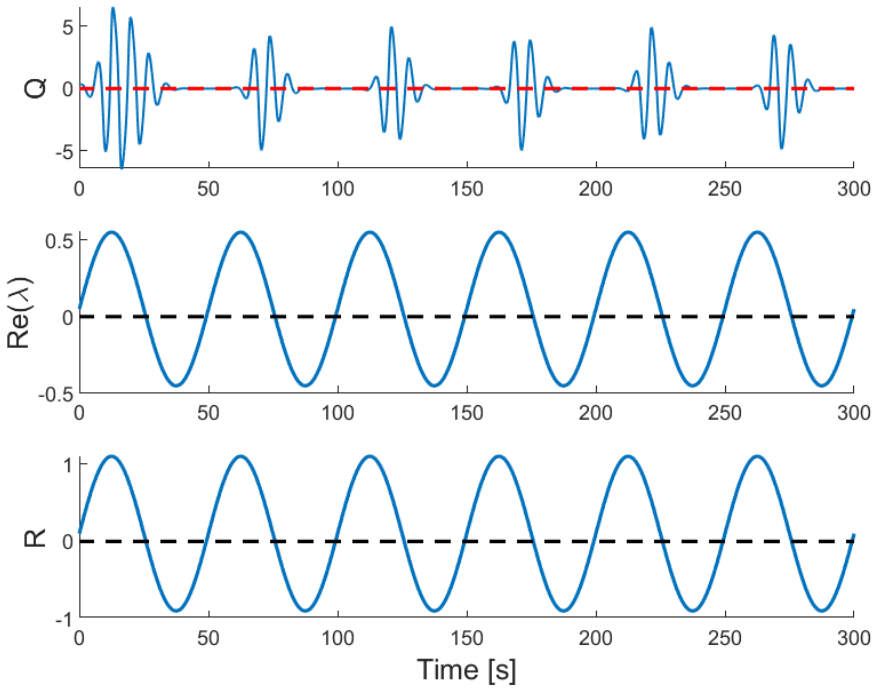

Figure 5.2: $A = 10$, $\bar{R} = 0.1$, $\tau = 50s$, $\omega_n = 1$. System response, real part of characteristic values, and control parameter of the VDP versus time.

It should be noted that in the three nonlinear systems studied here that exhibit periodic pulsation, the common trait between them is that the control parameter which governs the Hopf bifurcation is related to damping in the system. In the combustion model, the control parameter T_0 (the outer wall temperature) essentially governs the overall heat loss in the system and serves to either damp or drive oscillations in the system. In the Van der Pol oscillator, the control parameter R is the resistance in the circuit, which governs damping in the oscillations of the system as well as the shape of the limit cycle. The control parameter μ in the Simple Hopf Bifurcation model serves as a damping mechanism, although that system was constructed purely to produce a relatively simple limit cycle.

5.2 Arrhythmias in the Van der Pol Oscillator

Similarly to the SHB model, the VDP with periodic pulsation can exhibit arrhythmias in the system response. As we shall see, the type of bifurcation that leads to arrhythmias is identical in both systems: the characteristic values of the central fixed point periodically (but temporarily) switch from a complex-conjugate pair to a pair of real values.

To begin, some variables will be defined for the sake of brevity in the derivation.

$$B = \sin(\frac{2\pi}{\tau}t)$$

$$R^{'} = \bar{R}(1 + AB)$$

The Jacobian for the VDP system of Eqn. 5.1 is then:

$$[J] = \begin{bmatrix} 0 & 1 \\ -2QU - \omega_n^2 & R^{'} - Q^2 \end{bmatrix} \tag{5.2}$$

Evaluating the Jacobian at the central fixed point $Q^* = U^* = 0$ and solving for the characteristic values (the eigenvalues of the Jacobian), the following expression is obtained for the fixed point's two characteristic values:

$$\lambda_{1,2} = \frac{\bar{R}}{2}(1 + AB) \pm \frac{1}{2}\sqrt{\bar{R}^2(1 + AB)^2 - 4\omega_n^2} \tag{5.3}$$

Which are always a complex conjugate pair when the argument of the square root is negative. In order to find the bifurcation point(s), when the characteristic values change from a complex conjugate pair into a pair of real numbers, the times at which the argument of the square root becomes positive must be determined. In other words, the bifurcation points can be determined using the following equation:

$$(R^{'})^2 - 4\omega_n^2 = 0 \tag{5.4}$$

Next, the expression for $R^{'}$ is substituted back into Eqn. 5.4, and expanding the square term and rearranging the equation yields:

$$B^2 + \frac{2}{A}B + \left(\frac{1}{A^2} - \frac{4\omega_n^2}{A^2\bar{R}^2}\right) = 0 \tag{5.5}$$

Now applying the quadratic equation to solve for B and simplifying gives:

$$B = -\frac{1}{A} \pm \frac{2\omega_n^2}{A\bar{R}} \tag{5.6}$$

This implies that since B is a function of time, and has upper and lower bounds of +1 and -1, respectively, the bifurcations will occur at the discrete times when B is equal to one of these extrema. Also, for a given value of $\bar{R}$ the values of A at which the bifurcations occur can be determined. For example: taking $\bar{R} = 0.1$ as before, the values of A at which the bifurcations will occur are given by the following two expressions (one expression for each extremum):

$$+1 = -\frac{1}{A} \pm \frac{20}{A} \tag{5.7}$$

$$-1 = -\frac{1}{A} \pm \frac{20}{A} \tag{5.8}$$

Which yields four possible bifurcation points for A: ± 19 and ± 21. The analysis will be restricted to $A > 0$, as using the bifurcation points for $A < 0$ gives different transient behavior in the trajectory, but identical curves for the characteristic values in the complex plane (the negative sign on the bifurcation points simply implies a phase shift of π in B). In general, the effect of each bifurcation point on the characteristic values is:

$$A \geq \frac{2\omega_n}{\bar{R}} - 1 \implies \lambda_1,\, \lambda_2 \in \mathbb{R}, \quad \text{once per cycle in interval } \Delta t_1 \tag{5.9}$$

$$A \geq \frac{2\omega_n}{\bar{R}} + 1 \implies \lambda_1,\, \lambda_2 \in \mathbb{R}, \quad \text{twice per cycle in intervals } \Delta t_1 \;\&\; \Delta t_2 \tag{5.10}$$

Obviously the above equations imply that the two bifurcation points are always separated by a value of 2 (the diameter of the unit circle) in the parameter A. Looking at the plots in Fig. 5.3, we see the evolution of the characteristic value curves in the complex plane – as well as the effects on the pulsation behavior – as A increases and passes through these bifurcation points. Notice that although the arrhythmia bifurcations appear clearly in the plots of the characteristic values, their effect on the system response is subtle. This is due to the brief time interval in which the arrhythmias appear when A is near the bifurcation points. In fact only at amplitudes much larger than the bifurcation values do the arrhythmias show a strong effect on the system response; such a case can be seen in Figs. 4.6b and 4.7b of the Simple Hopf Bifurcation. Of course, this implies that the Van der Pol oscillator cannot exhibit a case when the single arrhythmia is strongly apparent in the system response by itself, as the largest amplitude possible before the next arrhythmia appears is only greater than the first bifurcation point by a value of 2.

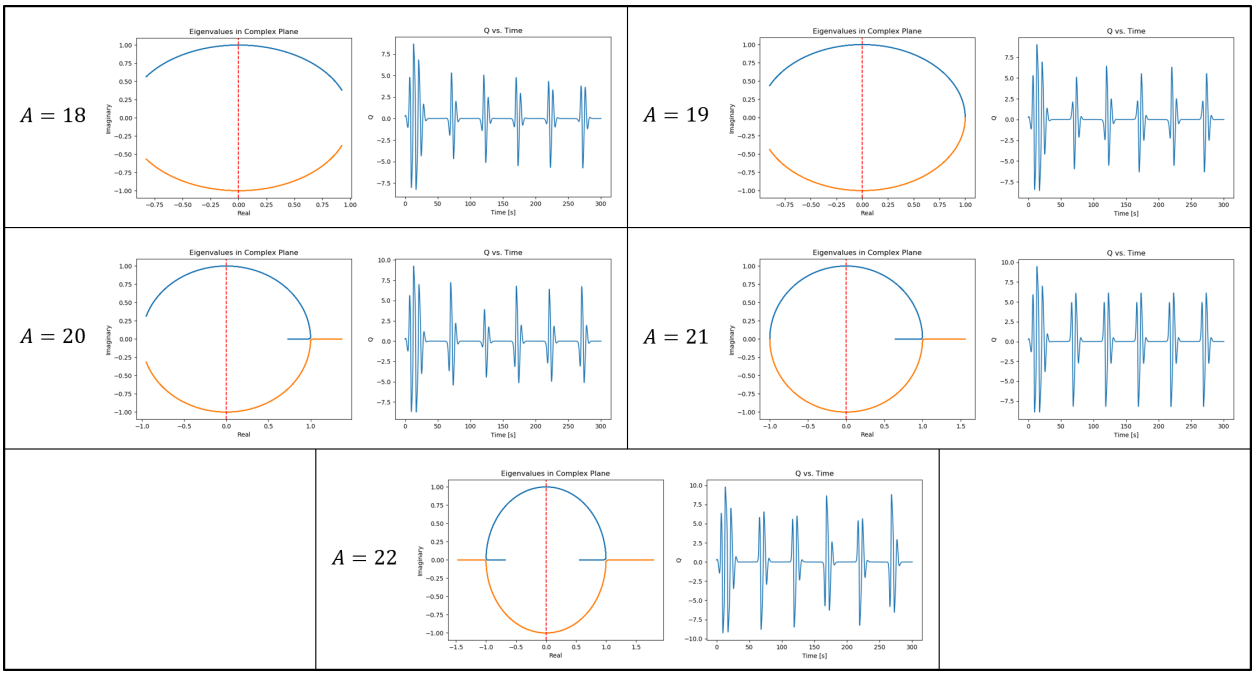

Figure 5.3: $\tau = 50s$, $\bar{R} = 0.1$, $\omega_n = 1$. Evolution of arrhythmia bifurcations in the periodic pulsation pattern of the Van der Pol oscillator as the forcing amplitude, A, is increased.

In order to determine the time intervals when each of the two arrhythmias occurs, Eqns. 5.7 and 5.8 are rewritten as the inequalities which they truly are.

$$B \geq -\frac{1}{A} + \frac{2\omega_n}{AR} \tag{5.11}$$

$$B \leq -\frac{1}{A} - \frac{2\omega_n}{AR} \tag{5.12}$$

From these equations, the two arrhythmia constants k_1 and k_2 will be defined as:

$$k_1 = -\frac{1}{A} + \frac{2\omega_n}{AR} \qquad\qquad k_2 = -\frac{1}{A} - \frac{2\omega_n}{AR}$$

Now Eqns. 5.11 and 5.12 can be rewritten as:

$$\sin(\frac{2\pi}{\tau}t) = B \geq k_1 \tag{5.13}$$

$$\sin(\frac{2\pi}{\tau}t) = B \leq k_2 \tag{5.14}$$

The equalities of the above two equations can be used to determine the precise times, t_1 and t_2, when the arrhythmia bifurcations occur (and when the time intervals, Δt_1 and Δt_2, begin). From these two times, the angular constants ϕ_1 and ϕ_2 can also be defined – as was done with the SHB.

$$t_1 = \frac{\tau}{2\pi}\sin^{-1}(k_1) \qquad\qquad t_2 = \frac{\tau}{2\pi}\sin^{-1}(k_2)$$

$$\phi_1 = \sin^{-1}(k_1) = \frac{2\pi}{\tau}t_1 \qquad\qquad \phi_2 = \sin^{-1}(k_2) = \frac{2\pi}{\tau}t_2$$

The intervals (both angular and temporal) in which the arrhythmias will be present can be determined using these constants. Looking at the first arrhythmia, $B \geq k_1$ only when:

$$\phi_1 \leq \frac{2\pi}{\tau}t \leq \pi - \phi_1 \quad \text{or} \quad t_1 \leq t \leq \frac{\tau}{2} - t_1$$

And looking at the second arrhythmia, $B \leq k_2$ only when:

$$\pi + \phi_2 \leq \frac{2\pi}{\tau} t \leq 2\pi - \phi_2 \quad \text{or} \quad \frac{\tau}{2} + t_2 \leq t \leq \tau - t_2$$

The angular intervals can be described using the following diagram. Note that when A has a value such that only the first arrhythmia appears, the shaded interval between 0 and π would be present in the diagram but the shaded interval between π and 2π would not be present.

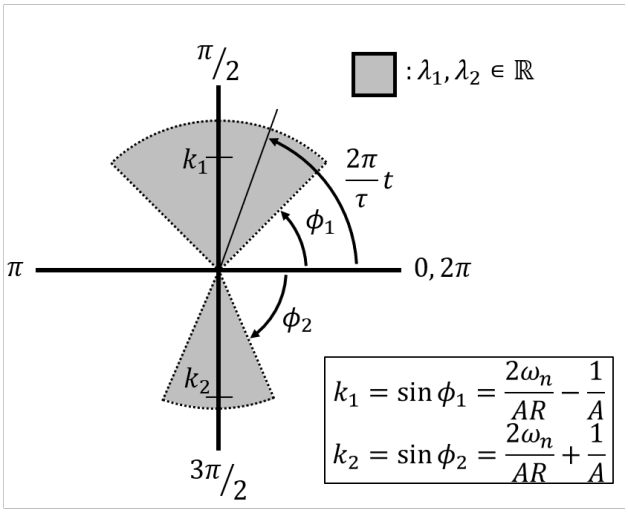

Figure 5.4: Visualization of the angular intervals where λ_1 and λ_2 are real in the VDP.

In short, the time intervals in which each of the two arrhythmias appear as well as the specific times at which those intervals begin are given in Eqns. 5.15 and 5.16.

$$\Delta t_1 = \frac{\tau}{2} - 2t_1 \ , \quad t_1 = \frac{\tau}{2\pi} \sin^{-1}(k_1) \ ; \quad \text{w/ intervals beginning at: } \ t = n\tau + t_1 \ , \quad n = 0, 1, 2, 3, ... \tag{5.15}$$

$$\Delta t_2 = \frac{\tau}{2} - 2t_2 \ , \quad t_2 = \frac{\tau}{2\pi}\sin^{-1}(k_2) \ ; \quad \text{w/ intervals beginning at: } \ t = \left(n + \frac{1}{2}\right)\tau + t_2 \ , \quad n = 0, 1, 2, 3, ... \tag{5.16}$$

The form of these equations is the same as that in the arrhythmia of the SHB (see Eqn. 4.23), with the major difference being the expression for the arrhythmia constant, k.

CHAPTER 6

QUASI-PERIODIC BEHAVIORS

Although we refer to the phenomenon as periodic pulsation (due to the periodic behavior of characteristic values that cause the pulsation, and the visual periodicity of pulses), the trajectory behavior is generally quasi-periodic – barring arrhythmias. This is evidenced by the existence of drift rings in the Poincaré planes of periodic pulsation signals, as well as the shape of frequency spectra in the Discrete Fourier Transforms (DFT) of periodic pulsation signals.

6.1 Toroids and Drift Rings

As with most two-frequency systems, it is useful to plot the state space trajectory on the surface of a torus, with the major radius corresponding to the slow frequency (the forcing frequency in periodic pulsation) and the minor radius corresponding to the fast frequency (the natural frequency in periodic pulsation). The transformation from state space to a torus is straightforward, and is done using the following equations:

$$x = (R_o + x_1)\cos(\omega_{slow}t) \tag{6.1}$$

$$y = (R_o + x_1)\sin(\omega_{slow}t) \tag{6.2}$$

$$z = x_2 \tag{6.3}$$

where (x,y,z) are Cartesian coordinates, x_1 and x_2 are the state parameters of the system, and R_o is the major (outer) radius of the torus. The time variable t can be thought of as the third state space parameter, as periodic pulsation systems are generally autonomous (dependent on time). Essentially all that is happening with this transformation is that you are wrapping the pulsation that occurs in the 3-D (t,x_1,x_2) state space (see Fig. 6.1) onto a torus based on the slow forcing period, such that the pulses overlap. Some example toroids for each of three dynamic systems studied is given in Fig. 6.2 below.

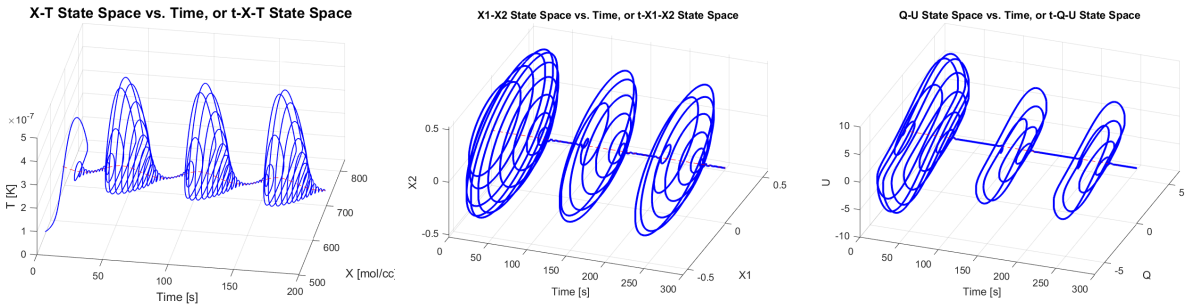

(a) Combustion model (b) SHB (c) VDP

Figure 6.1: Example periodic pulsation signals for each system plotted in the (t,x_1,x_2) space.

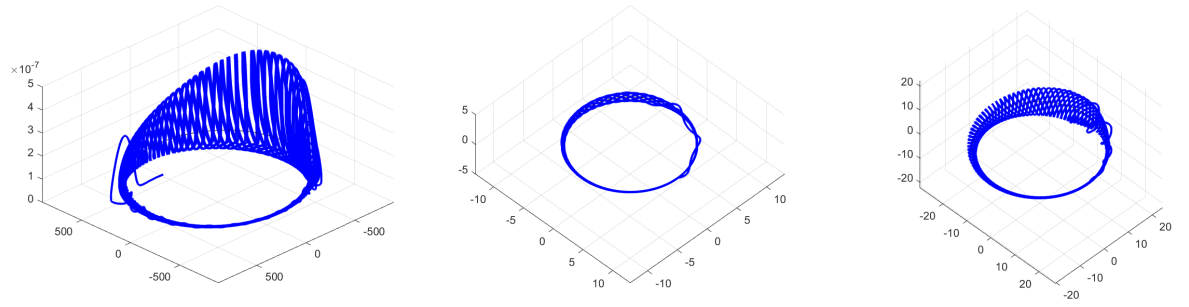

(a) Combustion model (b) SHB (c) VDP

Figure 6.2: Example periodic pulsation signals plotted as toroids for each system. The transient phase usually appears as a section of the trajectory outside the steady-state toroid.

Now if many pulses are plotted for each of the three systems, it eventually appears that the trajectory completely fills the surface of the toroid. This behavior is also analyzed by taking a Poincaré plane of the toroid; in other words, we take an angular slice outwards from the center of the toroid at some angle (any angle will do in this case). Every slow forcing period, the trajectory will pass just once through the Poincaré plane. If enough forcing periods (pulses) are plotted, it will appear that the intersection points on the Poincaré plane eventually fill in a solid ring – a drift ring. This is a telltale sign that a system is quasi-periodic. Example drift rings for each of the three systems are given in Fig.6.3 below.

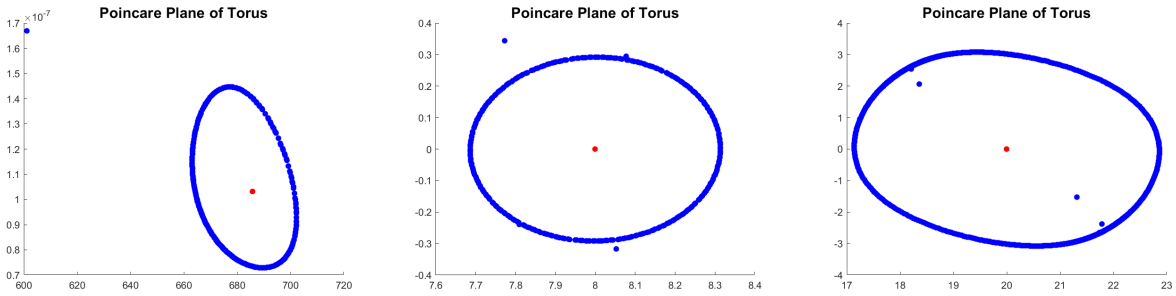

(a) Combustion model (b) SHB (c) VDP

Figure 6.3: Poincaré planes of periodic pulsation signals in each system. The transient phase appears as outlier points not on the drift ring.

6.2 Discrete Fourier Transform

The Discrete Fourier Transform (DFT) gives several insights into the frequency behavior of periodic pulsation. The DFT is determined through the following integral transformation, although the integral is computed numerically at discrete frequencies:

$$f(\omega) = \int_{-\infty}^{\infty} f(t) e^{-2\pi\omega j t} d\omega \tag{6.4}$$

where $f(t)$ is a trajectory for a given state variable, x. The frequency responses of periodic pulsation signals have several interesting aspects related to quasi-periodicity. In general – and barring arrhythmias – there is a spread of frequencies in the Fourier spectrum (a "frequency comb"), with a strong peak at the natural frequency. The slow forcing frequency also does not usually appear as a peak in the spectrum due to quasi-periodicity. Essentially, if you pick a point on a given pulse, and move over one forcing period to the next pulse, that point will not have the same value; this is the reason the Fourier transform does not generally detect the forcing frequency.

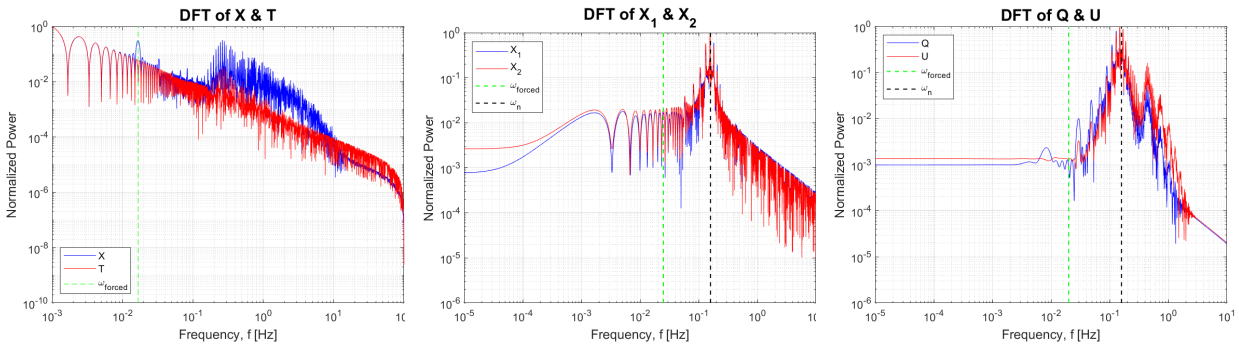

(a) Combustion model (b) SHB (c) VDP

Figure 6.4: Example DFT's of periodic pulsation signals in each system. The black dashed line represents the natural frequency of the system, and the green dashed line represents the forcing frequency.

For periodic pulsation signals, it is common to see power at frequencies much lower than the forcing frequency. This is also partly due to quasi-periodicity. As before, if one were to pick a given point somewhere on the trajectory, and then advance along the time axis for one forcing period, the trajectory value would not be the same due to quasi-periodicity; however, that does not mean the value will not be repeated *at all* at some random later time. The Fourier transform picks up on these longer periods, hence the power at very low frequencies. This low-frequency effect is magnified for strong periodic pulsation, i.e. pulses with nearly flat lines in between.

The frequency spectrum of the forced Combustion model has some distinct features that distinguish it from the other two models:

- The natural frequency cannot be marked as a single value; in fact, Yang & Gray showed that the natural frequency of the system depends directly on the value of T_0 [9]. Since the value of T_0 is constantly changing in our forced version of the combustion model, the natural frequency is also constantly changing.

- The forcing frequency often *does* show up as pronounced peak in the Fourier spectrum. The reason for this is that central fixed point itself changes periodically in time, not just its characteristic values. This is in contrast to the SHB and VDP systems, where the central

fixed point does not change with time, but its characteristic values do change with time.

6.3 Effects of Arrhythmias

Normally, the trajectory behavior of periodic pulsation is actually quasi-periodic. However, if a system can exhibit arrhythmias (such as the SHB and VDP systems), the trajectory behavior can switch to periodic if the arrhythmias are present. In essence, the arrhythmias can "reset" the pulses and return them to the same trajectory path every forcing period. This is easier to visualize by looking at the bifurcation diagrams for forcing amplitude in the SHB and VDP in Figs. 6.5 and 6.6. The bifurcation diagrams were generated by sampling periodic pulsation signals at the natural frequency of each system for many values of forcing amplitude. For both diagrams, every value of A/A_{bif} has 125 sample points plotted.

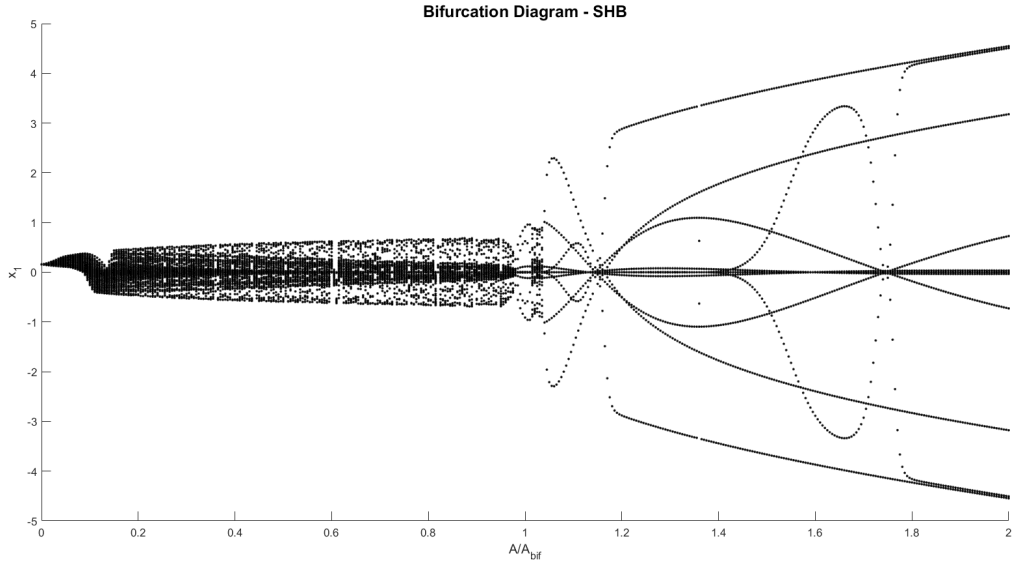

Figure 6.5: Bifurcation diagram for the SHB. x_1 is plotted against A/A$_{bif}$ (forcing amplitude normalized by the amplitude at which arrhythmias appear). $\bar{\mu} = 0.05$, $\tau_f/\tau_n = 10$.

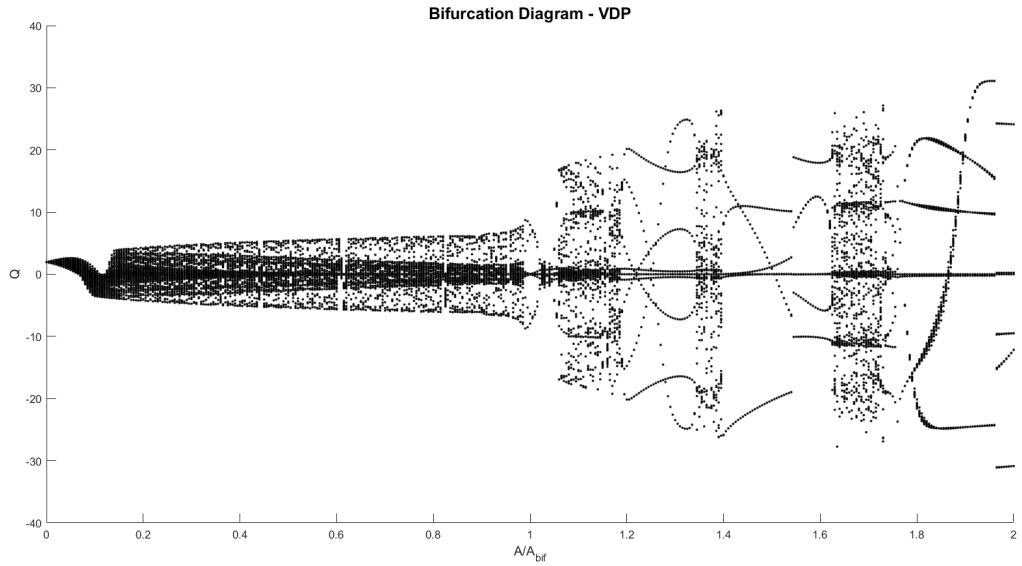

Figure 6.6: Bifurcation diagram for the VDP. Q is plotted against A/A$_{bif}$ (forcing amplitude normalized by the amplitude at which the first arrhythmia appears). $\bar{R} = 0.1$, $\tau_f/\tau_n = 10$.

Several interesting observations can be made about these arrhythmia bifurcation diagrams. The first and most important observation is that up to the first arrhythmia ($A/A_{bif} = 1$), both the VDP and SHB systems exhibit a very similar quasi-periodic pattern. Both systems even show "gaps" (regions closer to periodic behavior) at similar values of A/A_{bif}, most prominently around 0.35, 0.6, and 0.8. The exact dynamical cause of these gaps is unknown. The second observation is that the trajectory behavior starts to become periodic just *before* the arrhythmia value of $A/A_{bif} = 1$ is reached in both systems. This seems to occur around A/A_{bif} values of 0.980 and 0.990 for the SHB and VDP, respectively. The third observation is the presence of apparently chaotic bands in the arrhythmia region $A/A_{bif} \geq 1$ in both systems. It appears that the SHB has only one chaotic band just after the arrhythmias appear, whereas the VDP has several large chaotic bands in the arrhythmia region. This may be due to the relative complexity/nonlinearity of the VDP compared to the SHB. The fourth observation has to do with “amplitude switching” in the arrhythmia region of the VDP. This refers to the abrupt change in sign of the trajectory amplitudes, most notably around A/A_{bif} values of 1.540 and 1.960. The dynamical cause of this “amplitude switching” is

unknown, but it stands in stark contrast to the symmetry and relative smoothness of the arrhythmia region of the SHB.

It should be noted that bifurcation diagrams could be generated for the forcing period instead of the forcing amplitude (i.e. holding A constant and varying τ). Doing so would simply produce a long pattern similar to the common pre-arrhythmia pattern in Figs. 6.5 and 6.6.

CHAPTER 7

OTHER DYNAMICAL CURIOSITIES

While studying each of the three nonlinear dynamic systems in this work, it became apparent that a relatively simple function can reproduce periodic pulsation – which we be rightfully called the "Pulsation Function". Although producing even a steady-state closed form solution for any of the previous three systems using the function proved fruitless, the function itself serves as the simplest form of pulsation that was found. Along similar lines, we were also able to produce periodic pulsation in the simple spring-mass-damper system (with its own peculiar issues), although that system could not be solved using the Pulsation Function, either.

7.1 The Pulsation Function

The Pulsation Function serves as the simplest function that we have found capable of reproducing periodic pulsation, and was constructed by keeping in mind the criteria for periodic pulsation determined from the three nonlinear systems studied here. The function is as follows:

$$f(t) = Ae^{\sin(\omega_2 t+\phi_2)-1}\sin(\omega_1 t + \phi_1), \quad \omega_2 < \omega_1 \tag{7.1}$$

where A is the maximum amplitude of the pulses, ω_1 and ω_2 are the fast and slow modes, respectively, and ϕ_1 and ϕ_2 are the phase angles of the sine waves of both modes. The (-1) in the argument of the exponential serves to normalize the maximum of the exponential term to a value of 1, and gives maximum amplitude control strictly to the value of A. An example of the function is given in Fig. 7.1 below

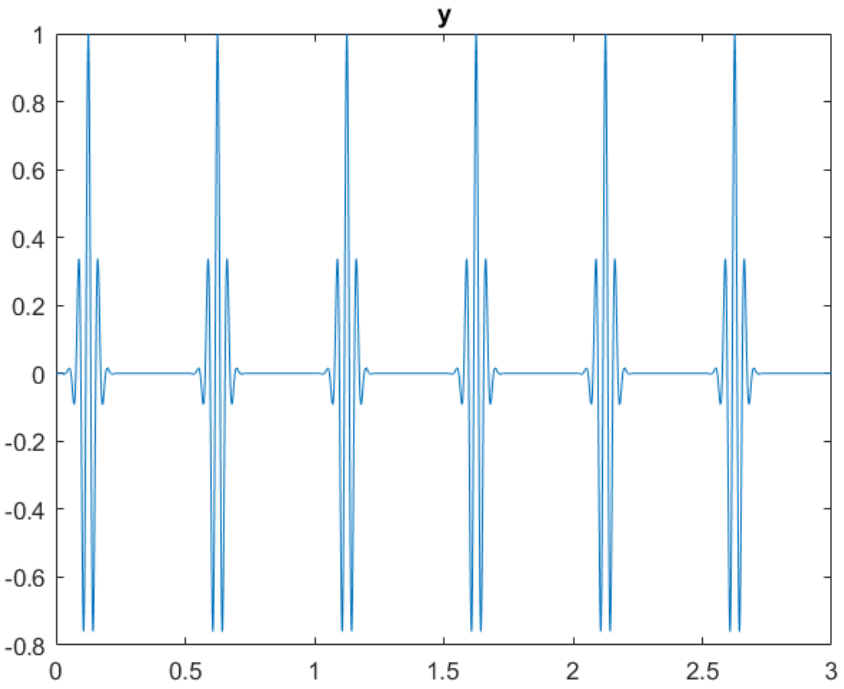

Figure 7.1: Pulsation Function for values of the parameters: $A = 1, \omega_1/\omega_2 = 13, \phi_1 = \phi_2 = 0$

Unlike the three nonlinear systems studied before, this function follows the normal rules for quasi-periodic (or ergodic) behavior; that is to say, if the frequency ratio $\alpha = \omega_1/\omega_2$ is a rational number (i.e. the frequencies are commensurate), then the function is strictly periodic, but if the frequency ratio is an irrational number (i.e. the frequencies are incommensurate), then the function is quasi-periodic.

$$\begin{cases} \alpha \in \mathbb{Q} \implies \text{Periodic} \\ \alpha \in (\mathbb{R} - \mathbb{Q}) \implies \text{Quasi-Periodic} \end{cases} \tag{7.2}$$

It is important to note that this function does not exhibit a true limit cycle, at least when we consider its state space representation, f and df/dt; in essence this function only models a central fixed point switching from a spiral node to a spiral repellor and back. In that regard it may hold promise for modeling trajectories in nonlinear systems with trajectories near the central fixed point, but our attempts at using the Pulsation Function to solve nonlinear periodic pulsation systems have

proved fruitless (likely due to the lack of a limit cycle component to the function).

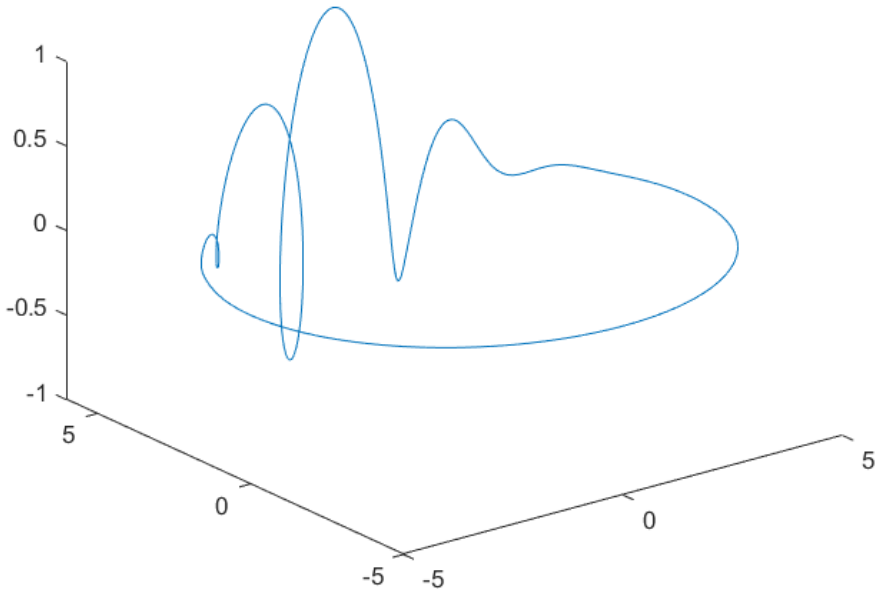

Figure 7.2: Example toroid representation of the Pulsation Function. The state space variables are f and its first derivative df/dt. $A = 1$, $\omega_1/\omega_2 = 13$, $\phi_1 = \phi_2 = 0$

7.1.1 Pulsation vs. Beating

It is also important to make the distinction between periodic pulsation and acoustic beating. Acoustic beating is defined through the following equation:

$$f(t) = A[\cos(\omega_1 t) + \cos(\omega_2 t)], \qquad \omega_1 \approx \omega_2 \tag{7.3}$$

Beating is simply a summation of sine waves with similar frequencies, while periodic pulsation has an exponential with an oscillatory argument. This is what allows periodic pulsation to have apparently flat lines between its pulses; acoustic beating cannot achieve such behavior. A visual comparison between the Pulsation Function and acoustic beating is given in Fig. 7.3 below.

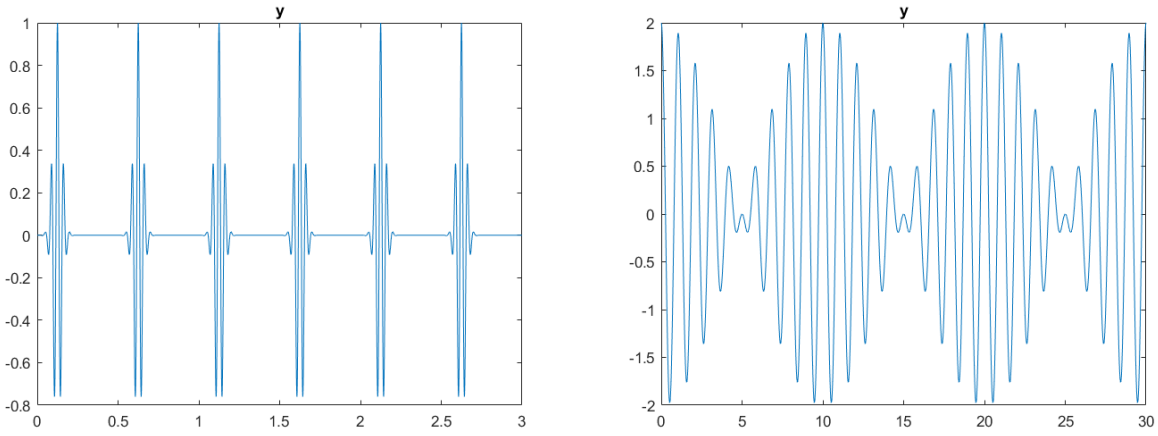

(a) Pulsation Function

(b) Acoustic beating

Figure 7.3: Comparison between the Pulsation Function and acoustic beating.

7.1.2 Pulse Symmetry

One final point of interest regarding the Pulsation Function has to do with pulse symmetry and patterns, and it stems from variation in the frequency ratio, $\alpha = \omega_1/\omega_2$. Looking only at integer values of α: if α is even each pulse is symmetric, while if α is odd each pulse is anti-symmetric. However, similar state space patterns repeat for every increase by 4 in α; for example, in Fig. 7.4, the state space for $\alpha = 14$ is similar in pattern to $\alpha = 10$, but with an additional loop in the center around the fixed point at (0,0).

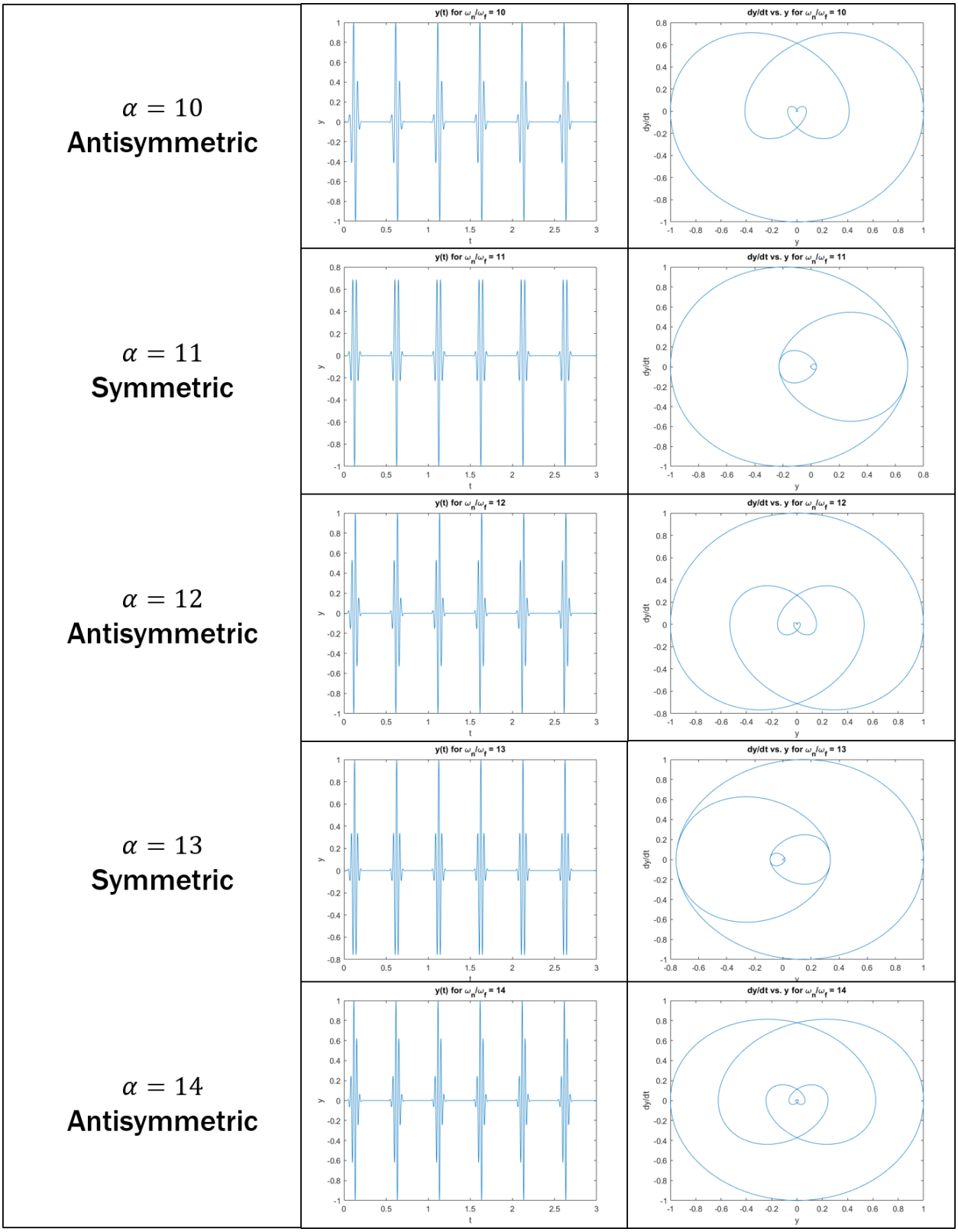

Figure 7.4: Example evolution of the Pulsation Function as the frequency ratio ($\alpha = \omega_1/\omega_2$) increases by integer values.

7.2 Periodic Pulsation in the Spring-Mass-Damper

The idea that the damping parameter might govern periodic pulsation led to attempts to produce it in a spring-mass-damper system. The basic differential equation has the same general form, except the damping term has a periodic forcing associated with it. Adding the periodic forcing changes the nature of the differential equation. The normal spring-mass-damper is a linear time-invariant (LTI), or linear autonomous, differential equation with a well known solution form, but the forced version in Eqn. 7.4 below changes the differential equation to a linear time-variant (LTV), or linear non-autonomous, equation without a known analytical solution.

$$m\ddot{y} + \bar{\gamma}(1 + A\sin(\omega_f t))\dot{y} + ky = 0 \tag{7.4}$$

where m is the mass, k is the spring constant, and $\bar{\gamma}$ is the average damping coefficient. Note that the natural frequency is still given by $\omega_n = \sqrt{k/m}$. The form of the forcing term is the same (for now) as that used in the nonlinear systems, i.e. $(1 + A\sin(\omega_f t))$. Defining $z = \dot{y}$, we convert Eqn. 7.4 to a system of coupled first-order equations:

$$\begin{cases} \dot{z} = -\frac{\bar{\gamma}(1+AB)}{m} z - \frac{k}{m} y \\ \dot{y} = z \end{cases} \quad , \qquad B \equiv \sin(\omega_f t) \tag{7.5}$$

Again we have defined B for the sake of brevity. This system has one fixed point at (y,z) = (0,0). It can be shown that the characteristic values of this fixed point are given by Eqn. 7.6 below.

$$\lambda_{1,2} = -\frac{\bar{\gamma}}{2m}(1 + AB) \pm \frac{1}{2}\sqrt{\frac{\bar{\gamma}^2}{m^2}(1 + AB)^2 - 4\frac{k}{m}} \tag{7.6}$$

Note that Eqn. 7.6 is identical in form to that of Eqn. 5.3 in the VDP; this means the characteristic values in both systems move on identically shaped paths in the complex plane, and suggests that the spring-mass-damper might exhibit two arrhythmia bifurcations like the VDP. We shall see that while arrhythmias do exist in the spring-mass-damper when looking at the characteristic

values, how they affect the system is fundamentally different. For this system to possibly produce periodic pulsation, we know that λ_1, λ_2 must form a complex-conjugate pair (barring arrhythmias). This will only occur when the argument of the square root is negative, or:

$$\frac{\bar{\gamma}^2}{m^2}(1+AB)^2 - 4\frac{k}{m} < 0 \tag{7.7}$$

This inequality allows us to determine the maximum forcing amplitude for which the system might exhibit periodic pulsation. The maximum value of B is +1, so we will use this value in Eqn. 7.7 to determine the absolute maximum for A. We could also look at the minimum for A by using the minimum value of B, -1, but this will yield a negative forcing amplitude; for simplicity we will restrict ourselves to A > 0. Substituting B=+1 and rearranging, the inequality for the maximum forcing amplitude is given by:

$$A < \frac{1}{\bar{\gamma}}\sqrt{4km} - 1 = \frac{2m\omega_n}{\bar{\gamma}} - 1 = A_{max} \tag{7.8}$$

However, it turns out that even when this inequality is satisfied, the numerical solution to the spring-mass-damper does not give periodic pulsation. Instead it produces pulses that either damp out or grow exponentially with time, as can be seen in Fig. 7.5.

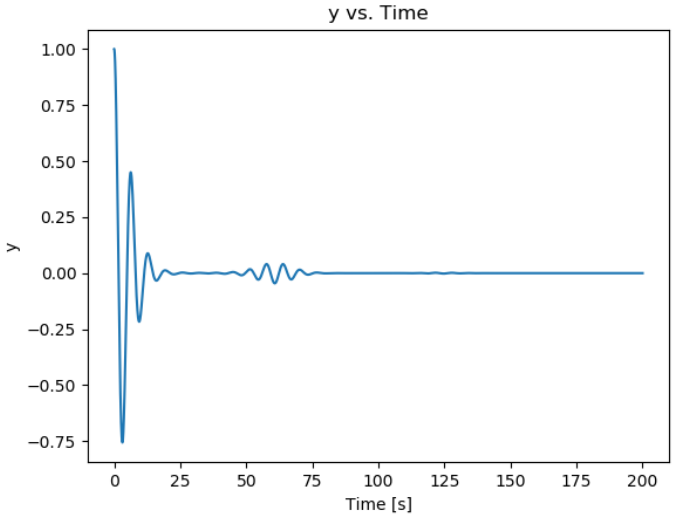

Figure 7.5: Spring-mass-damper system with forcing term 1+AB. Pulses appear, but are dominated by overall exponential decay. $A = 5$, $\bar{\gamma} = 0.1$, $\omega_n/\omega_f = 10$, $k = m = \omega_n = 1$.

The culprit behind this overall damping/forcing behavior is the form of the forcing term, specifically the 1 in the term (1+AB). This 1 multiplies with the damping coefficient such that it dominates the long-term behavior of the solution. Therefore it stands to reason that if we change the form of the forcing term from (1+AB) to simply (AB), we should produce periodic pulsation in the spring-mass-damper (as the term causing overall exponential growth/decay has been removed). Indeed this is the case, as we shall soon see. The new differential equation appears as follows:

$$m\ddot{y} + \bar{\gamma}(AB)\dot{y} + ky = 0, \qquad B \equiv \sin(\omega_f t) \tag{7.9}$$

which again has a single fixed point at $(y, \dot{y}) = (0, 0)$. However, the equation for the characteristic values of this fixed point becomes:

$$\lambda_{1,2} = -\frac{\bar{\gamma}}{2m}(AB) \pm \frac{1}{2}\sqrt{\frac{\bar{\gamma}^2}{m^2}(AB)^2 - 4\frac{k}{m}} \tag{7.10}$$

which is *nearly* identical in form to Eqn. 4.8, meaning the characteristic values in the complex

plane now behave more like the SHB, rather than the VDP. This suggests that, like the SHB, there is now only one value of A for which an arrhythmia could appear. Periodic pulsation should occur in the spring-mass-damper up to that value; this is expressed by the following:

$$A < \frac{1}{\bar{\gamma}}\sqrt{4km} = \frac{2m\omega_n}{\bar{\gamma}} = A_{max} \tag{7.11}$$

Indeed, with the new form for the spring-mass-damper given by Eqn. 7.9, periodic pulsation can be produced. An example periodic pulsation solution (computed numerically) is given in Fig. 7.6.

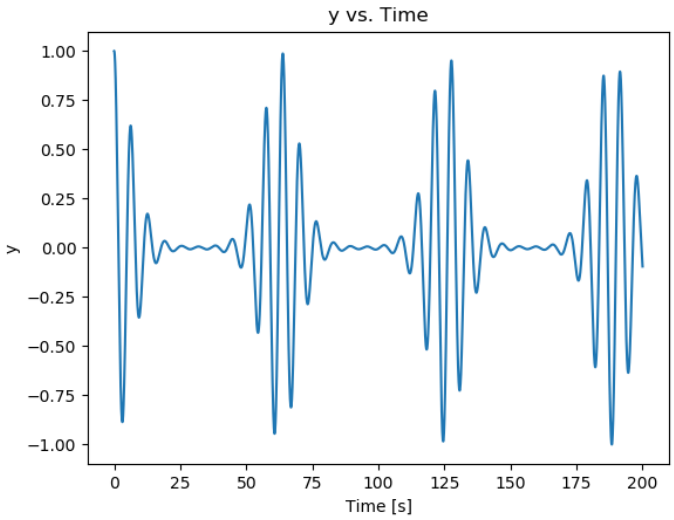

Figure 7.6: Spring-mass-damper system with forcing term AB. The system exhibits periodic pulsation. $A = 5$, $\bar{\gamma} = 0.1$, $\omega_n/\omega_f = 10$, $k = m = \omega_n = 1$.

The fact that periodic pulsation can be generated at all in the spring-mass-damper system provides one *very* important observation: periodic pulsation is not strictly limited to nonlinear systems. It should be restated that both of the two criteria we developed previously in Section 1.4 for periodic pulsation apply to nonlinear systems; however, only the second criteria is needed for linear systems, i.e. periodic forcing with a frequency less than the natural frequency is sufficient to

produce periodic pulsation. In other words, for a given linear system, all that is required to produce periodic pulsation is a slow periodic forcing on the damping parameter such that the real part of the characteristic values of the central fixed point switches back and forth between positive and negative. Therefore, it appears that periodic pulsation can only occur in linear time-variant (LTV) systems.

The absence of a limit cycle in linear systems does have its consequences, however. For instance, if $A \geq A_{max}$ (which would normally be the arrhythmia bifurcation point in nonlinear systems), then when the characteristic values become a pair of positive real values the solution will eventually blow up and experience unbounded exponential growth away from the fixed point (for an example, see Fig. 7.7 below). In the nonlinear systems, this unbounded growth away from the fixed point is eventually curbed by the reappearance of a stable limit cycle.

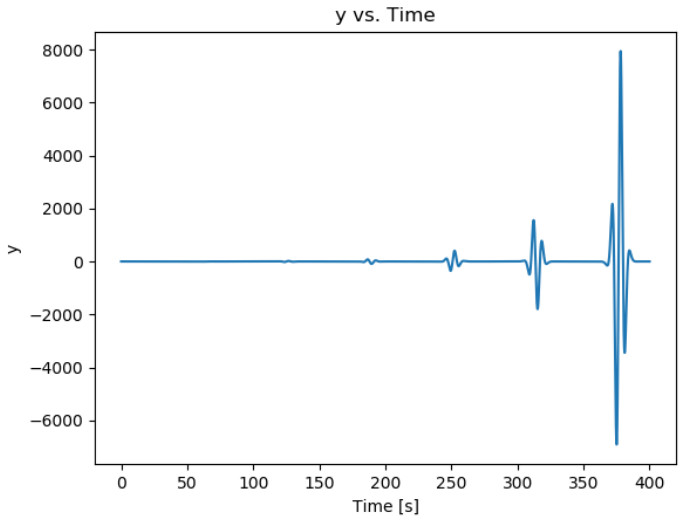

Figure 7.7: Spring-mass-damper experiencing unbounded exponential growth in pulse amplitude. The forcing amplitude is equal to its maximum value, the point where nonlinear systems would normally experience arrhythmias. $A = A_{max} = 20$, $\bar{\gamma} = 0.1$, $\omega_n/\omega_f = 10$, $k = m = \omega_n = 1$.

Also, we have found that if the frequency ratio ω_n/ω_f in the spring-mass-damper is too large, this can also cause unbounded exponential growth. This is most likely due to the characteristic

values spending too much time on the right side of the imaginary axis, where Re(λ)>0. We have yet to determine the exact value of the frequency ratio for which this apparent bifurcation occurs.

7.2.1 Notes on the Spring-Mass-Damper

Upon inspection of the state space $(y, \dot{y})$, as well as y and $\dot{y}$ versus time for the spring-mass-damper exhibiting periodic pulsation (see Fig. 7.8), it appears that the trajectory behavior is quasi-periodic. If this is indeed the case, then that suggests the quasi-periodic nature of trajectories in periodic pulsation is not necessary only related to the linearity or nonlinearity of a system, but instead has a more fundamental dynamical cause. A more likely reason has to do with the motion of characteristic values in the complex plane causing continuous and periodic change in the frequency of a system. For the Combustion model, it is easy to see that the frequency of the system (how far the characteristic values are from the origin of the complex plane) changes drastically in time. For the SHB, VDP, and spring-mass-damper, the characteristic values move along the edge of a circle in the complex plane. However, in each of these systems the center of that circle is offset to the right or left of the origin of the complex plane; this means the distance from the characteristic values to the origin is not constant in time, and therefore the frequency of the system is not constant – just like in the Combustion model (but less immediately apparent upon inspection).

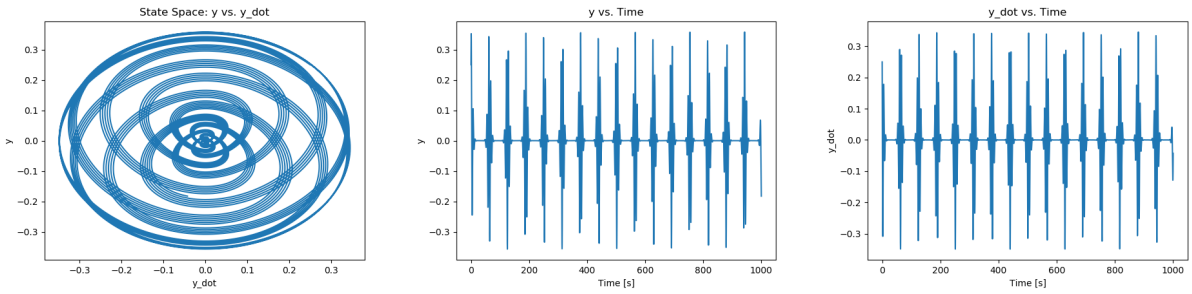

(a) y vs. $\dot{y}$ (b) y vs. t (c) $\dot{y}$ vs. t

Figure 7.8: State space, y, and $\dot{y}$ plots for the spring-mass-damper showing signs of quasi-periodicity. $A = 10$, $\bar{\gamma} = 0.1$, $\omega_n/\omega_f = 10$, $k = m = \omega_n = 1$.

CHAPTER 8

DISCUSSION AND CONCLUSIONS

In general – but especially in the case of the Combustion model – the periodic pulsation phenomenon can be thought of as oscillation between overall generation and overall dissipation of energy in a given system. It follows that the driving factor, then, should be a parameter connected to the system damping. This applies clearly to each of the systems studied. For example: in the Combustion model, this parameter was the wall temperature T_0, which directly affects the heat loss/ energy dissipation of the system; in the Van der Pol oscillator, R was the resistance/damping parameter of the system derived from the circuit; in the Simple Hopf Bifurcation, μ was related to damping; and obviously in the spring-mass-damper γ was the damping coefficient. Of course, for nonlinear systems, when the generation is greater than the dissipation the system can remain bounded due to the appearance of a limit cycle. In the case of the Combustion model, however, the explosion limits place restrictions on the largest possible amounts of energy generation or dissipation. There may still be a region where a limit cycle exists (as was shown), but this region is bounded on one end by an explosion limit.

In terms of physical applications, the Combustion model, the Van der Pol oscillator, and the spring-mass-damper are the models based on physical systems (thermokinetic, electrical, and mechanical, respectively). The SHB is the only one that does not really have a physical analogue, as it was constructed purely to model a limit cycle and Hopf bifurcation. Out of all the models, however, the Combustion model stands alone as the only model truly constrained by its physical nature. For instance, its fast frequency is strictly governed by the chemical kinetics and reaction rates, whereas in the other models the fast frequency is simply a parameter that can be arbitrarily chosen.

There is at least one major issue with the Combustion model studied here in respect to accurately modeling experimental observations: the time scale of this model is far too slow compared to that seen in the Hong, *et al.* experiment [1]. The pulsation behavior appears to be the same,

but the frequencies of the experiment are much higher and on the scale of the combustion chamber resonance ($\sim$200Hz). This suggests that the dynamical mechanisms of periodic pulsation (Hopf Bifurcation, slow mode on the damping parameter, etc.) are likely present, but the correct low-order set of equations with the proper timescales to describe the behavior is still missing. It is obvious that the fast-mode natural frequency is related to the combustion chamber resonance, but the problem arises in identifying the particular damping mechanism that is driving the pulsation. Heat loss is the most likely suspect, but viscous properties, acoustic damping, mass transport, and other dissipation phenomena have not been entirely ruled out. This time scale problem is not really an issue for the SHB, VDP, and spring-mass-damper, as the natural frequency in those systems is a value that can be arbitrarily chosen. In the Combustion model, the fast frequency at which the system oscillates is determined by the kinetic rates of each of the sub-reactions altogether with the heat loss – the frequency is not just a variable that we can easily adjust.

As far as CFD simulation is concerned, we have at least been able to generate flame holding using the Jones & Lindstedt mechanism for the combustion of methane and air in our simulated swirl combustor. We have so far only been able to achieve this using the stoichiometric O/F ratio, but have been successful in doing so in both the steady state and transient solutions. It cannot be overstated how crucial the axisymmetric assumption was in reducing the problem complexity, and therefore computation time. Because of that assumption, the dimensionality of our simulations was essentially 2D+time with a 4-step reaction mechanism; the simulation time at most was about 2 days for a transient simulation with a large number of time steps. Without the axisymmetric assumption, our simulation would have to be 3D+time (if the injector was not an annulus, but a set of discrete orifices, for instance), and the time is necessary since periodic pulsation is a transient phenomenon. If there were no chemical reactions, then a 3D+time fluid simulation alone could take on the order of several days to complete, but then if we add back in the 4-step reaction mechanism to our simulation, the computation time for a single transient run could be on the order of weeks. This massive increase in computation time due to complex chemical reaction mechanisms is the reason that complex fluid simulations like LES or DNS can typically only afford a 1-step chemical

reaction, or none at all. The fact that our simulations can be treated as 2D+time allows us the freedom to use more complex chemical reaction mechanisms and keep the computation time down to reasonable amounts.

In terms of the dynamics of each system, it appears that the requirements of quasi-periodicity (incommensurate frequencies, etc.) cannot readily be applied to periodic pulsation due to non-constant frequencies in the system. Regardless, it seems the phenomenon is in general quasi-periodic because of that same fact. When looking at the power spectrum for each system, instead of clearly defined peaks for the natural and forcing frequencies, there is actually a spread of frequencies. This is most likely due to the characteristic values moving in time in the complex plane and therefore changing the frequency at which the trajectory orbits the central fixed point. This is especially accurate when the trajectory is near to either the spiral node or the limit cycle. The Combustion model in particular has a strongly time-dependent natural frequency, since not only do the characteristic values change in time, but that system's natural frequency directly depends on the value of T_0 which – for periodic pulsation – we have made to oscillate in time [9]. The quasi-periodicity also shows up as drift rings in the Poincaré plane taken once every slow forcing period for a given periodic pulsation signal.

One other point of interest is the arrhythmia bifurcation discussed in the SHB and VDP systems. To reiterate, an arrhythmia bifurcation in periodic pulsation systems occurs when the characteristic values of the central fixed point periodically switch back and forth from a complex-conjugate pair to a pair of real values. Looking at the central fixed point alone, when the characteristic values are a complex-conjugate pair the fixed point is a spiral node or spiral repellor and the trajectory orbits the fixed point. When the characteristic values are real the fixed point is a simple node or simple repellor and the trajectory no longer orbits the fixed point, but instead moves directly towards or away from the fixed point. One important observation is that the time interval in which the arrhythmias exist (and the characteristic values ar real) takes the same form for both the SHB and the VDP (see Equations 4.23, 5.15, and 5.16). The difference between the two models is the expression for the arrhythmia constant, k, which in both systems is a function of the average

control parameter value, denoted here by $\bar{\mu}$, the forcing amplitude A, and the natural frequency ω_n.

$$k = f(\bar{\mu}, A, \omega_n)$$

Previously we discussed that the spring-mass-damper cannot exhibit arrhythmias in the same sense as the nonlinear systems. For the spring-mass-damper, if $A \geq A_{bif}$, then the system blows up through unbounded exponential growth. However, there could be a connection between that behavior and the Combustion model, which blows up for $A > 0.05$. The parallel we are drawing here is between the "arrhythmia" of the spring-mass-damper and the explosion limits of the Combustion model. Although the characteristic values for both systems travel on completely different paths in the complex plane, both systems blow up for some critical value of A.

We have shown that with proper forcing of heat loss, we can use a reduced-order Combustion model to generate periodic pulsation that is similar to the pattern seen in the experiment of Hong *et al.* [1]. We have also had some success in combustion modeling by CFD, where we use a 4-step reaction mechanism for methane to generate a transient flame in an axisymmetric swirl combustor of the same dimensions as the Hong *et al.* experiment.

We have shown that periodic pulsation can be produced in three different nonlinear dynamical systems – a reduced-order Combustion model, the Simple Hopf Bifurcation model, and the Van der Pol oscillator – and one linear dynamical system – the spring-mass-damper. Two criteria have been developed for nonlinear systems that determine if periodic pulsation can be produced:

1. The system must exhibit a Hopf Bifurcation for some range of control parameter values.

2. There must be some periodic forcing on the control parameter, with a frequency lower than that of the natural frequency of the system.

For linear systems, only the second criteria is necessary and sufficient for periodic pulsation.

REFERENCES

[1] J. G. Hong, K. C. Oh, U. D. Lee, and H. D. Shin, "Generation of low-frequency alternative flame behavior in a lean premixed combustor," *Energy & Fuels*, vol. 22, no. 5, pp. 3016–3021, 2008.

[2] J. M. Diels, J. J. Fontaine, I. C. McMichael, and F. Simoni, "Control and measurement of ultrashort pulse shapes (in amplitude and phase) with femtosecond accuracy," *Applied Optics*, vol. 24, no. 9, pp. 1270–1282, 1985.

[3] T. C. Lieuwen, "Experimental investigation of limit-cycle oscillations in an unstable gas turbine combustor," *Journal of Propulsion and Power*, vol. 18, no. 1, pp. 61–67, 2002.

[4] T. Lieuwen, Y. Neumeier, and B. T. Zinn, "The role of unmixedness and chemical kinetics in driving combustion instabilities in lean premixed combustors," *Combustion Science and Technology*, vol. 135, no. 1-6, pp. 193–211, 1998.

[5] F. Weng, M. Zhu, and L. Jing, "Beat: a nonlinear thermoacoustic instability in rijke burners," *International Journal of Spray and Combustion Dynamics*, vol. 6, no. 3, pp. 247–266, 2014.

[6] F. Weng, D. Zhong, and M. Zhu, "Influence of dynamic bifurcations on beating oscillations in a rijke burner," 2015.

[7] D. M. Newitt and L. S. Thornes, "The oxidation of propane. part i. the products of the slow oxidation at atmospheric and at reduced pressures," *Journal of the Chemical Society (Resumed)*, pp. 1656–1665, 1937.

[8] D. M. Newitt and W. G. Schmidt, "The oxidation of propane. part ii. the products of the slow oxidation at high pressures," *Journal of the Chemical Society (Resumed)*, pp. 1665–1669, 1937.

[9] C. H. Yang and B. F. Gray, "Slow oxidation of hydrocarbons and cool flames," *The Journal of Physical Chemistry*, vol. 73, no. 10, pp. 3395–3406, 1969.

[10] R. C. Hilborn, *Chaos and Nonlinear Dynamics: An Introduction for Scientists and Engineers*. New York, NY: Oxford University Press, 1994.

[11] B. Van Der Pol and J. Van Der Mark, "Lxxii. the heartbeat considered as a relaxation oscillation, and an electrical model of the heart," *The London, Edinburgh, and Dublin Philosophical Magazine and Journal of Science*, vol. 6, no. 38, pp. 763–775, 1928.

[12] B. Glaz, I. Mezić, M. Fonoberova, and S. Loire, "Quasi-periodic intermittency in oscillating cylinder flow," *Journal of Fluid Mechanics*, vol. 828, pp. 680–707, 2017.

[13] J. Redondo, G. J. de Valcárcel, and E. Roldán, "Intermittent and quasiperiodic behavior in a zeeman laser model with large cavity anisotropy," *Physical Review E*, vol. 56, no. 6, p. 6589, 1997.

[14] H. Herzel, P. Plath, and P. Svensson, "Experimental evidence of homoclinic chaos and type-ii intermittency during the oxidation of methanol," *Physica D*, vol. 48, no. 2-3, pp. 340–352, 1991.

[15] S. W. Benson, "The kinetics and thermochemistry of chemical oxidation with application to combustion and flames," *Progress in Energy and Combustion Science*, vol. 7, no. 2, pp. 125–134, 1981.

[16] N. N. Semenov, "Gas explosions and the theory of chain reactions," *Physics-Uspekhi*, vol. 36, no. 4, pp. 279–287, 1993.

[17] N. N. Semenov, *Some Problems in Chemical Kinetics and Reactivity*. Princeton, NJ: Princeton University Press, 1959.

[18] I. Glassman, *Combustion*. Boston, MA: Academic Press, 4 ed., 2008.

[19] Y. Huang and V. Yang, "Dynamics and stability of lean-premixed swirl-stabilized combustion," *Progress in Energy and Combustion Science*, vol. 35, no. 4, pp. 293–364, 2009.

[20] W. Jones and R. Lindstedt, "Global reaction schemes for hydrocarbon combustion," *Combustion and flame*, vol. 73, no. 3, pp. 233–249, 1988.

[21] A. N. Karpetis, D. W. Ellis, and A. C. Bayeh, “Miniature supersonic burner for the study of combustion at extreme conditions. i: Internal flow,” *Journal of Energy Engineering*, vol. 144, no. 5, Article 04018057, 2018.

APPENDIX A

ALTERNATIVE DERIVATION FOR SHB ARRHYTHMIAS

In polar coordinates, the forced SHB system and its Jacobian can be written as:

$$\vec{f}(r,\theta) = \begin{cases} f_1 = \dot{r} = r\Big(\bar{\mu}\big(1 + AB\cos^2(\theta)\big) - r^2\Big) \\ f_2 = \dot{\theta} = \omega_n - \frac{1}{2}\bar{\mu}AB\sin(2\theta) \end{cases} \quad , \quad B = \sin\big(\frac{2\pi}{\tau}t\big) \tag{A.1}$$

$$[J] = \begin{bmatrix} \bar{\mu}\big(1 + AB\cos^2(\theta)\big) - 3r^2 & -r\bar{\mu}AB\sin(2\theta) \\ 0 & -\bar{\mu}AB\cos(2\theta) \end{bmatrix} \tag{A.2}$$

The forcing term, B, has made a correction to both the $\dot{r}$ and $\dot{\theta}$ polar equations previously derived. The reason for using a forced period τ in this case instead of some forcing frequency f has to do with determining a value for another fixed point, θ^*, which will be discussed later. If the μ value in the original $\dot{x}_2$ equation could instead have been forced, this would amount to a phase shift of $\pi/2$ applied to the $\cos^2\theta$ term of the $\dot{r}$ equation.

When determining the fixed points of the system, the system of two differential equations is set equal to 0, as follows:

$$r\Big(\bar{\mu}\big(1 + AB\cos^2(\theta)\big) - r^2\Big) = 0, \qquad B = \sin\Big(\frac{2\pi}{\tau}t\Big) \tag{A.3}$$

$$\omega_n - \frac{1}{2}\bar{\mu}AB\sin(2\theta) = 0, \qquad B = \sin\Big(\frac{2\pi}{\tau}t\Big) \tag{A.4}$$

Again, τ is the period of the slow forcing mode. The first equation, Eqn. A.3, gives the fixed point expressions for both the spiral node and limit cycle, respectively.

$$r_1^* = 0 \tag{A.5}$$

$$r_2^* = \sqrt{\bar{\mu}(1 + AB\cos^2\theta)} \tag{A.6}$$

However the second equation, Eqn. A.4, produces an additional fixed point, θ^*. This fixed point is of importance since its appearance corresponds to the arrhythmia in the system response. Solving for θ in Eqn. A.4 produces the following result for θ^*:

$$\theta^* = \frac{1}{2}\sin^{-1}\left(\frac{2\omega_n}{\bar{\mu}AB}\right) \tag{A.7}$$

From Equation A.7, the fixed point θ^* will only exist (i.e. have a *real number* value) when the argument of $\sin^{-1}$ is between -1 and +1. In other words, θ^* only appears when:

$$0 \leq \left|\frac{2\omega_n}{\bar{\mu}AB}\right| \leq 1 \tag{A.8}$$

However, a more useful form of the above inequality moving forward is:

$$|B| = \left|\sin\left(\frac{2\pi}{\tau}t\right)\right| \geq \left|\frac{2\omega_n}{\bar{\mu}A}\right| \geq 0 \tag{A.9}$$

Which cannot be satisfied for $B = 0$ (since $A \neq 0$ and $\bar{\mu} \neq 0$), which occurs at times $t = 0,\ \frac{n\tau}{2}\ \ (n = 1, 2, 3, ...)$. More generally, the inequality cannot be satisfied if B is "near enough" to 0, with "near enough" being defined by the value $|\frac{2}{\bar{\mu}A}|$. In other words, θ^* will not exist in the time intervals where $|B|$ is less than this value. To find the time intervals in which θ^* *does* exist, and hence when the arrhythmia appears, all that need be done is determine the time intervals in which the inequality of Equation 4.11 is satisfied. Rearranging Equation 22, we define a new time variable, t_0, as follows:

$$t_0 = \frac{\tau}{2\pi}\sin^{-1}\left(\left|\frac{2\omega_n}{\bar{\mu}A}\right|\right) \tag{A.10}$$

Which is real only when:

$$0 \leq \left|\frac{2\omega_n}{\bar{\mu}A}\right| \leq 1 \tag{A.11}$$

Or, for $A > 0$:

$$A \geq \left| \frac{2\omega_n}{\bar{\mu}} \right| \tag{A.12}$$

This gives us the critical value for A, or the bifurcation point for the arrhythmia to appear. Looking at the previous cases where $\bar{\mu} = 0.05$ and inserting that value into Equation 4.14, we recover the previously stated critical value of $A = 40$. When Equation 4.14 is satisfied, the time t_0 is real and therefore intervals of time will exist in each forcing period where θ^* is real (i.e. the arrhythmia appears). For the sake of brevity we now define the constant angle ϕ as:

$$\phi = \sin^{-1}\left(\left| \frac{2\omega_n}{\bar{\mu}A} \right| \right) \tag{A.13}$$

Which has the following two properties:

$$\lim_{A \to \infty} \phi = 0 \tag{A.14}$$

$$0 \leq \phi \leq \frac{\pi}{2} \tag{A.15}$$

Substituting this definition into Equation 4.12 produces:

$$t_0 = \frac{\tau}{2\pi}\phi \tag{A.16}$$

Now, from Equation 4.11, θ^* is real only when the following equation is satisfied:

$$|B| \geq \sin(\phi) = \left| \frac{2\omega_n}{\mu A} \right| \tag{A.17}$$

The exact times at which $|B| = \sin(\phi)$ correspond to the exact times when θ^* either appears or disappears. Since $B = \sin(\frac{2\pi}{\tau}t)$, these discrete times allow us to write both the angular intervals

and time intervals for which θ^* is real:

$$\begin{cases} \phi \leq \frac{2\pi}{\tau} t \leq \pi - \phi \\ \pi + \phi \leq \frac{2\pi}{\tau} t \leq 2\pi - \phi \end{cases} \tag{A.18}$$

$$\begin{cases} t_0 \leq t \leq \frac{\tau}{2} - t_0 \\ \frac{\tau}{2} + t_0 \leq t \leq \tau - t_0 \end{cases} \tag{A.19}$$

Another way to visualize this is to plot the angular intervals of Equation A.18. The shaded regions in the figure below represent the angular intervals where θ^* is real, with the system angle (the argument of sine in B) rotating about the origin with a frequency of $2\pi/\tau$.

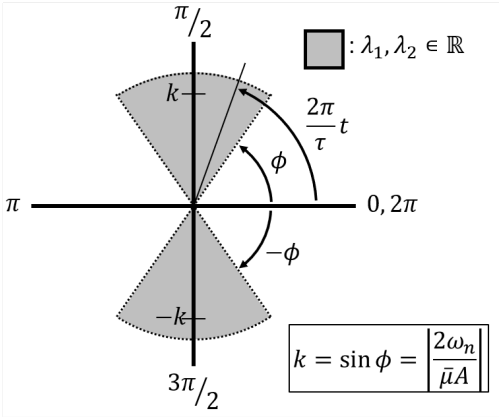

Figure A.1: Visualization of the angular intervals where θ^* is real.

While two arrhythmias must appear during each slow period according to Equation A.19 and Figure A.1, only one arrhythmia is visually apparent in the system response at the beginning of each pulse. The reason for this is that while there are two arrhythmias per slow period, one appears during the limit cycle phase and the other appears during the spiral node phase. The arrhythmia

that appears in the limit cycle phase is the one that appears at the beginning of each pulse. Looking at Figure 4.9 below in the subplot for the real part of the characteristic values, we see that there are indeed two arrhythmias per slow period; one during the limit cycle phase ($\mu > 0$) and one during the spiral node phase ($\mu < 0$). However, the limit cycle arrhythmia is much more apparent in the system response due to its drastically greater magnitude compared to the spiral node arrhythmia.

To summarize, this particular arrhythmia pattern is characterized by the periodic birth and death of an angular fixed point, as well as the periodic switching of the central fixed point's characteristic values from complex to real. It will only appear when the following two conditions are met (remembering that $B = \sin(\frac{2\pi}{\tau}t)$, and taking $A > 0$), and during the following time intervals, Δt:

$$1) \quad A \geq \left|\frac{2\omega_n}{\bar{\mu}}\right| \qquad\qquad 2) \quad |B| \geq \left|\frac{2\omega_n}{\bar{\mu}A}\right| = k$$

$$\Delta t = \frac{\tau}{2} - 2t_0, \quad \& \quad t_0 = \frac{\tau}{2\pi}\sin^{-1}(k) \;\; ; \;\; \text{w/ intervals beginning at: } \; t = \frac{n\tau}{2} + t_0, \;\; n = 0, 1, 2, 3... \tag{A.20}$$